This is a preprint, the final version is subject to change, of the American Mineralogist (MSA)
Cite as Authors (Year) Title. American Mineralogist, in press.
(DOI will not work until issue is live.) DOI: http://dx.doi.org/10.2138/am-2017-5891

Revision 1

Chlorine and fluorine partitioning between apatite and sediment melt at 2.5 GPa, 800°C: A new experimentally derived thermodynamic model

Huijuan Li[1*] and Joerg Hermann[1,2]

[1] Research School of Earth Sciences, Building 142, Mills Road, The Australian National University, Canberra, ACT 2601 Australia;

[2] Institute of Geological Sciences, Universität Bern, 3012 Switzerland

[*] Corresponding Author: huijuan.li@anu.edu.au

Abstract

The partitioning behaviour of Cl and F between apatite and sediment melt has been investigated by performing piston-cylinder experiments at 2.5 GPa, 800°C using a hydrous experimental pelite staring material (EPSM) with ~7 wt% H_2O and variable Cl (~0, 500, 1000, 2000, or 3000 ppm) and F (~0, 700, or 1500 ppm) contents, relevant for subduction zone conditions. Cl and F partitioning between apatite and melt is non-Nernstian, with $D_{Cl}^{Ap\text{-}melt}$ varying from 1.9-10.6 and $D_F^{Ap\text{-}melt}$ varying from 16-72. In contrast, Cl and F partition coefficients between phengite/biotite and melt ($D_{Cl}^{Phen\text{-}melt}$, $D_{Cl}^{Bi\text{-}melt}$, $D_F^{Phen\text{-}melt}$ and $D_F^{Bi\text{-}melt}$) were determined to be 0.24±0.01, 0.86±0.05, 1.4±0.1 and 3.7±0.4, respectively. The Nernstian partitioning of Cl and F between phengite/biotite and melt suggests ideal mixing of F, Cl and OH in phengite, biotite and melt.

Exchange coefficients for F, Cl and OH partitioning between apatite and melt were determined, with $K_{\mathrm{d}\,\text{Cl-OH}}^{\text{Ap-melt}}$ = 19-49, $K_{\mathrm{d}\,\text{F-OH}}^{\text{Ap-melt}}$ = 164-512, and $K_{\mathrm{d}\,\text{F-Cl}}^{\text{Ap-melt}}$ = 7-21. The evident variation of K_{d} values was attributed to non-ideal mixing of F, Cl and OH in apatite. A regular ternary solution model for apatite was developed by modeling the variation of K_{d} values for experiments from this study and those from Webster et al. (2009) and Doherty et al. (2014). Positive values (~15 to ~25 kJ/mol) obtained for Margules parameters $W_{\text{Cl-OH}}^{\text{Ap}}$, $W_{\text{F-Cl}}^{\text{Ap}}$ and $W_{\text{F-OH}}^{\text{Ap}}$ at low pressure conditions (0.2 GPa, 0.05 GPa and 900°C) are in contrast to zero or negative values at 2.5 GPa, 800°C. Based on a thermodynamic framework for F, Cl and OH exchange between apatite and melt, using values for $-\Delta_r G_{\text{Cl-OH}}^{\circ}(P,T)$, $-\Delta_r G_{\text{F-OH}}^{\circ}(P,T)$, $-\Delta_r G_{\text{F-Cl}}^{\circ}(P,T)$, $W_{\text{Cl-OH}}^{\text{Ap}}$, $W_{\text{F-Cl}}^{\text{Ap}}$ and $W_{\text{F-OH}}^{\text{Ap}}$ obtained through regression, F and Cl contents in melt can be derived from apatite compositions.

KEY WORDS: apatite, chlorine, exchange coefficient, fluorine, melt, partitioning, piston-cylinder experiments, regular solution model, subduction

1 Introduction

Apatite (referring to fluorapatite, chlorapatite, hydroxylapatite and solid solutions among them with the general formula, $Ca_5(PO_4)_3(OH,F,Cl)$), is the most abundant phosphate mineral on Earth and a ubiquitous accessory mineral in igneous, metamorphic and sedimentary rocks (Piccoli and Candela 2002; Spear and Pyle 2002; Hughes and Rakovan 2015). Apatite is also commonly found in extraterrestrial samples (e.g., Patiño Douce and Roden 2006; Jones et al. 2014). Apatite composition has been utilized as an indicator of volatile concentrations in ore-forming hydrothermal fluids (e.g., Boudreau

and McCallum 1989), mantle metasomatic agents (e.g., O'Reilly and Griffin 2000), metamorphic fluids (e.g., Harlov et al. 2006) and subduction zone fluids (e.g., Li and Hermann 2015); as a recorder of magmatic degassing history (e.g., Boyce and Hervig 2008); in modeling the initial volatile concentration in crystallizing felsic magma (e.g., Piccoli and Candela 1994), and as a probe for volatile concentrations in basaltic magmas and their source regions (e.g., Patiño Douce et al. 2011). In particular, OH in apatite has provided irrefutable evidence regarding the presence of H_2O on the Moon (e.g., Boyce et al. 2010, 2014; McCubbin et al. 2010a, 2010b; Greenwood et al. 2011; Barnes et al. 2013, 2014; Tartèse et al. 2013, 2014) and Mars (e.g., McCubbin et al. 2012; Gross et al. 2013; Howarth et al. 2015). Although the interpretation of volatile concentrations in fluid phases has been mainly qualitative or based on experimentally determined partition coefficients (*Ds*) (Brenan 1993; Mathez and Webster 2005; Webster et al. 2009; Doherty et al. 2014; Kusebauch et al. 2015), many researchers have recognized the non-Nernstian partitioning behaviour of F, Cl and OH between apatite and fluids and the necessity to use a thermodynamic formulism describing the F, Cl and OH exchange reaction between apatite and fluid (e.g., $K_{\mathrm{d}}^{\text{Ap-melt}}_{\text{Cl-OH}}$) for the purpose of quantifying volatile contents in fluid phases (Khorzhinskiy 1981; Zhu and Sverjensky 1991; Piccoli and Candela 1994, 2002; Patiño Douce et al. 2011; Boyce et al. 2014; Li and Hermann 2015; McCubbin et al. 2015).

Our previous experimental study (Li and Hermann 2015) investigated Cl partitioning between apatite and sediment melt with a synthetic experimental pelite starting material (EPSM) over a pressure and temperature range of 2.5-4.5 GPa and 690-900°C, appropriate for subducted slabs at sub-arc conditions. In addition to the *PT* dependence of

71 D_{Cl} between apatite and fluid phases, Li and Hermann (2015) also observed in a few
72 reconnaissance experiments a significant drop in D_{Cl} values with the addition of F into
73 the Cl-OH EPSM system. Although $K_d^{\text{Ap-melt}}_{\text{Cl-OH}}$ values showed greater consistency, the
74 difference between F-free and F-bearing systems was still evident.

75 In order to assess the compositional effect of F and Cl contents on K_d values, this study
76 carried out further experiments at fixed *PT* conditions of 2.5 GPa and 800°C with
77 variable Cl and F concentrations in the EPSM starting compositions. The compositional
78 characteristics of melt and mineral phases indicate that the variation of K_d values can be
79 attributed to the non-ideal mixing of F, Cl and OH in apatite. A regular ternary solution
80 model was developed for apatite within the thermodynamic framework of F, Cl and OH
81 exchange between apatite and melt. Such an apatite model will contribute to quantitative
82 and thermodynamic calibration of apatite as an indicator of F, Cl and H_2O content in fluid
83 phases.
84

85 ## 2 Experimental methods

86 ### 2.1 Starting material

87 The experimental pelite starting materials (EPSM, Table 1) have a major element
88 composition similar to both the average "Global Subducting Sediment" (GLOSS, Plank
89 and Langmuir 1998) and the average composition of upper continental crust (Taylor and
90 McLennan 1985; Rudnick and Gao 2003), but with variable Cl (~0, 500, 1000, 2000, or
91 3000 ppm) and F (~0, 700, or 1500 ppm) concentrations (Table 2). At the chosen *PT*
92 conditions of 2.5 GPa and 800°C, a H_2O content of ~7 wt% in EPSM produces a high
93 melt fraction of ~50-60%, with hydrous phases such as phengite remaining stable (Li and

Hermann 2015). The range of bulk F and Cl contents ensure F and Cl concentrations in melt are well below saturation (Webster and De Vivo 2002). The lower end of the bulk Cl range (~1.6% NaCl equivalent for EPSM-4, 6) is comparable to the salinity of fluid produced by high pressure antigorite breakdown (0.4-2 wt% $NaCl_{eq}$, Scambelluri et al. 2004), while lower F contents (~700 ppm) are similar to those of the upper continental crust (e.g., 557 ppm, Rudnick and Gao 2003). In addition, the starting materials were doped with trace elements at the 50-100 ppm level for the purpose of studying the Cl (and/or F) effect on trace element partitioning (results of which will be reported in a separate publication).

EPSM-1, 2, 3, 4, 5 and 6 were derived from the blending of three intermediate starting materials: a Cl and F-free hydrous composition with 7.20 wt% H_2O, and two anhydrous compositions with 2.90 wt% Cl, and ~1 wt% F respectively. EPSM-8, 9 and 10 were derived by blending three hydrous intermediate compositions: a Cl and F-free composition with 7.20 wt% H_2O, a Cl-bearing composition with 7.00 wt% H_2O and 2.69 wt% Cl, and a F-bearing composition with 7.09 wt% H_2O and ~1 wt% F. For each intermediate composition, major elements in the form of reagent grade oxides, carbonates and phosphates were combined and heated to 1000ºC to drive off volatiles. Fe was then added as synthetic fayalite. $Al(OH)_3$, NaCl and CaF_2 were added to the sintered mixture as the source of H_2O, Cl and F, respectively.

2.2 Experimental techniques

All piston-cylinder experiments were carried out at the Research School of Earth Sciences (RSES), The Australian National University. Gold capsules with a 2.3 mm

diameter were used in a ½ inch piston cylinder apparatus in combination with an assembly comprising of a MgO sleeve, graphite heater, salt sleeve and Teflon film. Temperature was monitored using type-B thermocouples ($Pt_{94}Rh_6/Pt_{70}Rh_{30}$) providing an accuracy of ±10°C. Pressures were converted directly from load and are accurate to 0.1 GPa. Rapid quenching was performed by cutting the power to the experiments. At the chosen *PT* conditions of 2.5 GPa and 800°C, hydrous EPSM compositions produce melts with buffered H_2O contents ~12 wt% (Li and Hermann 2015), which quench into bubble-free glasses (Fig. 1). As bubble-free glasses indicate no discernible degassing during experimental quenching, the F and Cl contents in bubble-free glasses can be considered representative of the F and Cl contents in melts at the experimental *PT* conditions.

2.3 Analytical techniques

The major element compositions of minerals and melts were determined using a JEOL 6400 SEM (Center of Advanced Microscopy, The Australian National University) with EDS operating at 15 kV, 1 nA beam current and 120 s counting time. While a focused beam was used for mineral analysis, a defocused beam was employed for glass analysis in order to minimize the Na and K loss. As a safe measure, we used only the Cl results from SEM EDS analysis which registered a value higher than 0.1 wt%, considering the high detection limit (0.03-0.05 wt%) for Cl. F analysis from SEM EDS was considered untrustworthy due to the overlapping of F *Kα*, Fe *Lα* and Mn *Lα* peaks. WDS analyses of Cl and F in hydrous minerals and melts were carried out using a Cameca SX-100 electron microprobe (EMP) operating at the Research School of Earth Sciences (RSES), The Australian National University. For the analysis of F in phengite, biotite and melt, a beam

setting of 20 nA current and 120 s counting time, combined with the use of a PC0 crystal in the spectrometer, was able to achieve a detection limit of 100±20 ppm. Constrained by the small grain size of apatites (1-5 μm), we chose to use a focused beam of 10 nA current and 20 s peak counting time, in order to limit the effect of F *K*α intensity variation during the analysis of F in apatite. By averaging a large data set (generally 20±5 data points), we were able to achieve an absolute standard deviation of 0.1-0.2 wt%, with the relative standard deviation less than 10%. Please refer to Li and Hermann (2015) for a detailed discussion regarding the analysis of F in apatite.

2.4 Mass balance calculations

A mass balance for major elements was performed to obtain the mass fraction of mineral and melt phases (Table 2), from which an estimate of Cl, F and H_2O content in melt was derived based on the mass balance of Cl, F and H_2O, for more details refer to Li and Hermann (2015). Such estimations provide a means to detect any volatile loss that may occur prior to, during or after the experiments. Error propagation indicates that the principle source of error in the calculation of Cl, F and H_2O contents in melt arises from the uncertainty in the estimated melt fraction. An estimated absolute error of ~10% for melt fraction results in an approximate 20% relative error for Cl, F and H_2O content in melt.

2.5. Exchange coefficients

Exchange coefficients for F, Cl and OH partitioning between minerals (apatite, phengite and biotite) and melt have been calculated. Using Cl-OH exchange between apatite and melt as an example, we can write the following exchange reaction:

$$Ca_5(PO_4)_3OH(Ap)+M_{1/x}Cl(melt)= Ca_5(PO_4)_3Cl(Ap)+ M_{1/x}OH(melt) \quad (1)$$

where $M_{1/x}Cl$ and $M_{1/x}OH$ represent two melt components containing any cation with a valance x. The exchange coefficient can then be defined as:

$$K_{d\,\text{Cl-OH}}^{\text{Ap-melt}} = \frac{X_{\text{Cl}}^{\text{Ap}} \times X_{\text{OH}}^{\text{melt}}}{X_{\text{OH}}^{\text{Ap}} \times X_{\text{Cl}}^{\text{melt}}} \quad (2)$$

where X_{Cl}^{Ap}, X_{OH}^{Ap}, X_{Cl}^{melt}, X_{OH}^{melt} are the mole fractions of Cl and OH in apatite and melt, respectively. An analogous formulism can be used to define Cl-OH, F-Cl, and F-OH exchange coefficients between any mineral (apatite, phengite or biotite) and melt. Hydrous silicate melt has been modeled as ideal mixtures of H_2O molecules (H_2O_m), OH, O, Cl and F following the work of Silver and Stolper (1985). And the equilibrium constant K_1 for the reaction H_2O_m (melt) + O (melt) = 2OH (melt), was calculated based on the model of ideal-mixing of H_2O species in rhyolitic melt at 2.83 GPa from Hui et al. (2008). The method for calculating mole fractions of Cl, OH and F in melt is detailed in the Appendix of Li and Hermann (2015).

Mole fractions of Cl and F in apatite are obtained from structural formula calculations, on the basis of 12.5 O^{2-}. Mole fractions of OH in apatite are calculated as $1-X_{Cl}^{Ap}-X_F^{Ap}$, assuming the halogen site is filled with F, Cl and OH only. In the case of phengite and biotite, the F, Cl and OH end-member components are taken as half the structural formula of 11 O^{2-}, for example, $(Na,K)_{0.5}(Mg,Fe,Al)(Al,Si,Ti)_2OH$, $(Na,K)_{0.5}(Mg,Fe,Al)(Al,Si,Ti)_2Cl$ and $(Na,K)_{0.5}(Mg,Fe,Al)(Al,Si,Ti)_2F$ representing the OH, Cl and F end-members of phengite respectively. The mole fractions of Cl and F in

phengite and biotite are calculated based on the structural formula of 11 O^{2-}, X_{Cl}=Cl(p.f.u.)/2, X_F=F(p.f.u.)/2, and the mole fractions of OH calculated as 1-X_{Cl}-X_F.

3 Results

The major mineral assemblages for experiments at 2.5 GPa, 800 ºC were always: Grt+Phen+Q+Ky (Table 2; Fig. 1). The only noticeable difference was the minor presence of biotite in some F-bearing experiments, which was attributed to the stabilization effect of F on biotite. Apatite, rutile and zircon were always present. Note that results for exp. C3269 with EPSM-1, exp. C3922 with EPSM-2 and exp. D1218 with EPSM-5 were previously reported in Li and Hermann (2015).

3.1 Melt composition

All melts were found to quench into bubble-free glasses (Fig. 1). SEM EDS analysis indicates all melts share a similar major element composition, with consistent analytical totals (Table 3). Normalized melt compositions are granitic with SiO_2 contents varying in a small range of 73.8 to 75 wt%. The molar ratios Si/Al and Na+K/Al are also similar among melts.

The Cl and F melt contents vary in ranges of 0.07-0.39 wt% and 0.02-0.15 wt%, respectively (Table 3). There is a good consistency between SEM EDS and EMP WDS Cl content analyses for melt (Fig. 2a). Also mass balance estimates show good agreement with analytical results (Fig. 2a), with the exception of exp. C4049, which has an analytical Cl content lower than that indicated by mass balance. Experiments reported in this study have been divided into three groups based on bulk F and Cl contents in the

starting compositions: "Cl", "Cl+700ppmF" and "Cl+1500ppmF". Cl content in melt shows a linear increase with the bulk Cl content in the EPSM starting materials, regardless of the bulk F content (Fig. 2b). Again exp. C4049 with EPSM-8 (~4000 ppm bulk Cl) appears as an outlier in Fig. 2b; with a melt Cl content lower than that estimated by simple extrapolation. There is reasonable agreement between EMP WDS analysis and mass balance estimates for F content in melt (Fig. 2c). As in the case of Cl, the analytical F content for melt from exp. C4049 is lower than the mass balance estimate (Fig. 2c). Such observations suggest that the actual bulk F and Cl contents in exp. C4049 are lower than intended. Although no attempts have been made to analyse the bulk F and Cl content for exp. C4049, both the mass balance using analysed Cl content in melt and the correlation between Cl content in melt and bulk Cl content (Fig. 2b) indicate an approximation of 3000 ppm for bulk Cl. The estimation of bulk Cl for exp. C4049 based on mass balance is calculated as: Cl_{bulk} (exp. C4049) = Cl_{bulk} (intended) – (C_{Cl}^{melt} (mass balance) - C_{Cl}^{melt} (SEM))* melt fraction. A similar estimate can also be made based on the correlation between apatite Cl content and bulk Cl (Fig. 3a, see next section). Based on both analytical and mass balance results, we can confirm that the F and Cl contents of bubble-free glasses are representative of F and Cl contents in melt at experimental conditions.

3.2 Apatite compositions

Apatites from all experiments have uniform major element compositions (Table 4), with P contents consistently ~3 (in p.f.u.), and Ca contents varying slightly between 4.6

and 4.8. With the exception of Si, all other major elements readily substitute for Ca in apatite.

Cl and F contents in apatite vary in the ranges 0.33-2.67 wt% and 1.57-2.49 wt%, respectively. The mole fraction of ClAp (X_{Cl}^{Ap}) increases linearly with the bulk Cl content in the starting composition, however, different linear trends are observed for the three data groups; and the slopes of these linear trends gradually decrease in the sequence "Cl", "Cl+700ppmF" and "Cl+1500ppmF" (Fig. 3a). Note that the data point for exp. C4049 falls on the trend defined by the other experiments when plotted with a corrected bulk Cl content of ~3000 ppm (Fig. 3a). The mole fraction of OHAp (X_{OH}^{Ap}) decreases with increasing bulk Cl content for the "Cl" data group; representing the exchange between Cl and OH in apatite. X_{OH}^{Ap} appears relatively constant within "Cl+700ppmF" and "Cl+1500ppmF" groups; indicating only exchange between F and Cl with the increase of bulk Cl content, with lower X_{OH}^{Ap} values corresponding to higher bulk F content (Fig. 3b). We therefore observe that the mole fraction of FAp (X_{F}^{Ap}) decreases with the increase of bulk Cl content (Fig. 3c).

3.3 Cl partitioning

Cl partition coefficients between apatite and melt ($D_{Cl}^{Ap\text{-}melt}$) have been determined for the three data groups "Cl", "Cl+700ppmF", and "Cl+1500ppmF", with values of 10.6±0.8, 3.5±0.2 and 1.9±0.2, respectively (Fig. 4a).

The Cl and F contents in phengite vary in the ranges 0.016-0.101 wt% and 0.04-0.22 wt%, respectively. Biotites have higher Cl and F contents with values in ranges 0.10-0.23 wt% and 0.30-0.60 wt% respectively. Due to the fact that Cl contents in phengite and

biotite also show linear correlation with the bulk Cl content as seen for melt (Table 5, 6), Cl partition coefficients between phengite and melt ($D_{Cl}^{Phen\text{-}melt}$) and biotite and melt ($D_{Cl}^{Bi\text{-}melt}$) are found to be independent of the bulk Cl and F contents, with values of 0.24±0.01 and 0.86±0.05, respectively (Fig. 4b). The Cl concentrations of all phases at equilibrium decrease in the sequence: apatite > melt > biotite > phengite.

3.4 F partitioning

The F content of mineral phases displays an increasing trend with the F content in melt (Fig. 5). F partition coefficients between phengite and melt ($D_{F}^{Phen\text{-}melt}$) and biotite and melt ($D_{F}^{Bi\text{-}melt}$) are determined to be 1.4±0.1 and 3.7±0.4, respectively (Fig. 5a). With the increase of F content in melt, F content in apatite displays a sharp increase, which then levels out (Fig. 5b). The resultant F partition coefficients ($D_{F}^{Ap\text{-}melt}$) vary in the range 16-72, showing a decreasing trend with increasing bulk F. The affinity for F uptake decreases in the sequence apatite > biotite > phengite > melt.

3.5 Exchange coefficients for F, Cl and OH partitioning

$K_{d\,Cl\text{-}OH}^{Ap\text{-}melt}$ values vary in the range 19-49, $K_{d\,F\text{-}OH}^{Ap\text{-}melt}$ has higher values in the range 164-512, while $K_{d\,F\text{-}Cl}^{Ap\text{-}melt}$ values are the smallest, ranging 7-21 (Table 4). The magnitude of such K_d values reflect the relative partitioning behaviour of F, Cl and OH between apatite and melt, where $D_{F}^{Ap\text{-}melt} > D_{Cl}^{Ap\text{-}melt} > D_{OH}^{Ap\text{-}melt}$. There is a notable decrease in $K_{d\,Cl\text{-}OH}^{Ap\text{-}melt}$ values for F-bearing experiments in comparison to F-free experiments.

Constant K_d values have been obtained for F, Cl and OH partitioning between phengite/biotite and melt, averaging 0.28±0.03, 6.1±1.3, 1.9±0.4, 1.18±0.11, 4.4±0.7,

5.2±1.1, for $K_{\mathrm{dCl\text{-}OH}}^{\mathrm{Phen\text{-}melt}}$, $K_{\mathrm{dF\text{-}Cl}}^{\mathrm{Phen\text{-}melt}}$, $K_{\mathrm{dF\text{-}OH}}^{\mathrm{Phen\text{-}melt}}$, $K_{\mathrm{dCl\text{-}OH}}^{\mathrm{Bi\text{-}melt}}$, $K_{\mathrm{dF\text{-}Cl}}^{\mathrm{Bi\text{-}melt}}$ and $K_{\mathrm{dF\text{-}OH}}^{\mathrm{Bi\text{-}melt}}$, respectively. The relative preference for F, Cl and OH can be interpreted as $D_{\mathrm{F}}^{\mathrm{Phen\text{-}melt}} > D_{\mathrm{OH}}^{\mathrm{Phen\text{-}melt}} > D_{\mathrm{Cl}}^{\mathrm{Phen\text{-}melt}}$ for phengite; and $D_{\mathrm{F}}^{\mathrm{Bi\text{-}melt}} > D_{\mathrm{Cl}}^{\mathrm{Bi\text{-}melt}} \geq D_{\mathrm{OH}}^{\mathrm{Bi\text{-}melt}}$ for biotite.

3.6 Modeling non-ideal mixing in apatite

For F, Cl and OH exchange between apatite and melt, the variation of K_{d} values is evident. Both the linear correlation between melt Cl content and bulk Cl content (regardless of varying bulk F content, Fig. 2b), and the invariant values of Cl and F partition coefficients between melt and phengite/biotite (Fig. 4b and 5a), suggest ideal-mixing of F, Cl and OH in melt, phengite and biotite. This is reasonable as both F and Cl represent trace elements in melt, phengite and biotite, and likely follow Henry's law, i.e., the activity of the element is proportional to its concentration. Therefore, we suggest that the observed variation in K_{d} values is a result of non-ideal mixing in the Cl-F-OH apatite solid solution. Based on the variation of K_{d} values, we are able to model the apatite ternary solution using Margules parameters, with results shown in Fig. 6 and summarized in Table 7. Note that linear regressions were performed using the data analysis function in Microsoft EXCEL.

For the Cl-OH exchange reaction between apatite and melt, we have

$$RT \ln K_{\mathrm{dCl\text{-}OH}}^{\mathrm{Ap\text{-}melt}} = -\Delta_r G_{\mathrm{Cl\text{-}OH}}^{\mathrm{o}}(P,T) - RT \ln(\gamma_{\mathrm{Cl}}^{\mathrm{Ap}} / \gamma_{\mathrm{OH}}^{\mathrm{Ap}}) \quad (3)$$

where $-\Delta_r G_{Cl-OH}^{\mathrm{o}}(P,T)$ is the negative Gibbs free energy for the exchange reaction at a given pressure and temperature, and $\gamma_{\mathrm{Cl}}^{\mathrm{Ap}}$, $\gamma_{\mathrm{OH}}^{\mathrm{Ap}}$ are the activity coefficients for ClAp and OHAp end-members, respectively.

297 Similarly we have the following relations for F-Cl and F-OH exchange reactions
298 between apatite and melt:

299 $$RT\ln K_{\mathrm{dF\text{-}Cl}}^{\mathrm{Ap\text{-}melt}} = -\Delta_r G_{\mathrm{F\text{-}Cl}}^{\mathrm{o}}(P,T) - RT\ln(\gamma_{\mathrm{F}}^{\mathrm{Ap}} / \gamma_{\mathrm{Cl}}^{\mathrm{Ap}}) \quad (4)$$

300 $$RT\ln K_{\mathrm{dF\text{-}OH}}^{\mathrm{Ap\text{-}melt}} = -\Delta_r G_{\mathrm{F\text{-}OH}}^{\mathrm{o}}(P,T) - RT\ln(\gamma_{\mathrm{F}}^{\mathrm{Ap}} / \gamma_{\mathrm{OH}}^{\mathrm{Ap}}) \quad (5)$$

301 We can model apatite as a regular ternary solution, with activity coefficients for apatite
302 end-members given as follows:

303 $$RT\ln\gamma_{\mathrm{Cl}}^{\mathrm{Ap}} = X_{\mathrm{OH}}^{\mathrm{Ap}}(1-X_{\mathrm{Cl}}^{\mathrm{Ap}})W_{\mathrm{Cl\text{-}OH}}^{\mathrm{Ap}} + X_{\mathrm{F}}^{\mathrm{Ap}}(1-X_{\mathrm{Cl}}^{\mathrm{Ap}})W_{\mathrm{F\text{-}Cl}}^{\mathrm{Ap}} - X_{\mathrm{OH}}^{\mathrm{Ap}}X_{\mathrm{F}}^{\mathrm{Ap}}W_{\mathrm{F\text{-}OH}}^{\mathrm{Ap}} \quad (6.1)$$

304 $$RT\ln\gamma_{\mathrm{OH}}^{\mathrm{Ap}} = X_{\mathrm{Cl}}^{\mathrm{Ap}}(1-X_{\mathrm{OH}}^{\mathrm{Ap}})W_{\mathrm{Cl\text{-}OH}}^{\mathrm{Ap}} + X_{\mathrm{F}}^{\mathrm{Ap}}(1-X_{\mathrm{OH}}^{\mathrm{Ap}})W_{\mathrm{F\text{-}OH}}^{\mathrm{Ap}} - X_{\mathrm{Cl}}^{\mathrm{Ap}}X_{\mathrm{F}}^{\mathrm{Ap}}W_{\mathrm{F\text{-}Cl}}^{\mathrm{Ap}} \quad (6.2)$$

305 $$RT\ln\gamma_{\mathrm{F}}^{\mathrm{Ap}} = X_{\mathrm{Cl}}^{\mathrm{Ap}}(1-X_{\mathrm{F}}^{\mathrm{Ap}})W_{\mathrm{F\text{-}Cl}}^{\mathrm{Ap}} + X_{\mathrm{OH}}^{\mathrm{Ap}}(1-X_{\mathrm{F}}^{\mathrm{Ap}})W_{\mathrm{F\text{-}OH}}^{\mathrm{Ap}} - X_{\mathrm{Cl}}^{\mathrm{Ap}}X_{\mathrm{OH}}^{\mathrm{Ap}}W_{\mathrm{Cl\text{-}OH}}^{\mathrm{Ap}} \quad (6.3)$$

306 where $W_{\mathrm{Cl\text{-}OH}}^{\mathrm{Ap}}$, $W_{\mathrm{F\text{-}Cl}}^{\mathrm{Ap}}$, $W_{\mathrm{F\text{-}OH}}^{\mathrm{Ap}}$ are the Margules parameters for F, Cl and OH mixing in
307 apatite.

308 By subtracting equation (6.2) from (6.1), we have

309 $$RT\ln(\gamma_{\mathrm{Cl}}^{\mathrm{Ap}} / \gamma_{\mathrm{OH}}^{\mathrm{Ap}}) = (X_{\mathrm{OH}}^{\mathrm{Ap}} - X_{\mathrm{Cl}}^{\mathrm{Ap}})W_{\mathrm{Cl\text{-}OH}}^{\mathrm{Ap}} + X_{\mathrm{F}}^{\mathrm{Ap}}(W_{\mathrm{F\text{-}Cl}}^{\mathrm{Ap}} - W_{\mathrm{F\text{-}OH}}^{\mathrm{Ap}}) \quad (7)$$

310 The consistency of $K_{\mathrm{d}\,\mathrm{Cl\text{-}OH}}^{\mathrm{Ap\text{-}melt}}$ values for F-free experiments supports the proposal by Li
311 and Hermann (2015) that the Cl-OH apatite binary solution can be treated as ideal, that is:

312 $$W_{\mathrm{Cl\text{-}OH}}^{\mathrm{Ap}} = 0 \quad (8)$$

313 Combining equations (3), (7) and (8) gives,

314 $$RT\ln K_{\mathrm{dCl\text{-}OH}}^{\mathrm{Ap\text{-}melt}} = -\Delta_r G_{\mathrm{Cl\text{-}OH}}^{\mathrm{o}}(P,T) + X_{\mathrm{F}}^{\mathrm{Ap}}(W_{\mathrm{F\text{-}OH}}^{\mathrm{Ap}} - W_{\mathrm{F\text{-}Cl}}^{\mathrm{Ap}}) \quad (9)$$

315 In plotting $RT\ln K_{\mathrm{dCl\text{-}OH}}^{\mathrm{Ap\text{-}melt}}$ versus $X_{\mathrm{F}}^{\mathrm{Ap}}$, the intercept of the linear regression is
316 $-\Delta_r G_{\mathrm{Cl\text{-}OH}}^{\mathrm{o}}(P,T)$; the slope gives the value for $W_{\mathrm{F\text{-}OH}}^{\mathrm{Ap}} - W_{\mathrm{F\text{-}Cl}}^{\mathrm{Ap}}$. As shown in Fig. 6a, the

317 regression results give a value of -34.03±0.49 kJ/mol for $\Delta_r G^{\circ}_{\text{Cl-OH}}(2.5\text{GPa}, 800°\text{C})$ and a

318 value of -10.48±1.11 kJ/mol for $W^{\text{Ap}}_{\text{F-OH}} - W^{\text{Ap}}_{\text{F-Cl}}$.

319 By subtracting equation (6.1) from (6.3), we have

320 $$RT\ln(\gamma^{\text{Ap}}_{\text{F}} / \gamma^{\text{Ap}}_{\text{Cl}}) = (X^{\text{Ap}}_{\text{Cl}} - X^{\text{Ap}}_{\text{F}})W^{\text{Ap}}_{\text{F-Cl}} + X^{\text{Ap}}_{\text{OH}}(W^{\text{Ap}}_{\text{F-OH}} - W^{\text{Ap}}_{\text{Cl-OH}}) \quad (10)$$

321 We know the following relation from the regression above,

322 $$W^{\text{Ap}}_{\text{F-OH}} - W^{\text{Ap}}_{\text{F-Cl}} = -10.48 \pm 1.11\text{kJ/mol} \quad (11)$$

323 Combining equations (4), (8), (10) and (11) gives

324 $$RT\ln K^{\text{Ap-melt}}_{\text{dF-Cl}} = -\Delta_r G^{\circ}_{\text{F-Cl}}(P,T) + (X^{\text{Ap}}_{\text{F}} - X^{\text{Ap}}_{\text{Cl}} - X^{\text{Ap}}_{\text{OH}})W^{\text{Ap}}_{\text{F-Cl}} + X^{\text{Ap}}_{\text{OH}} \times 10.48\text{kJ/mol} \quad (12)$$

325 By defining a variable

326 $$Y' = RT\ln K^{\text{Ap-melt}}_{\text{dF-Cl}} - X^{\text{Ap}}_{\text{OH}} \times 10.48\text{kJ/mol} \quad (13)$$

327 we have

328 $$Y' = -\Delta_r G^{\circ}_{\text{F-Cl}}(P,T) + (X^{\text{Ap}}_{\text{F}} - X^{\text{Ap}}_{\text{Cl}} - X^{\text{Ap}}_{\text{OH}})W^{\text{Ap}}_{\text{F-Cl}} \quad (14)$$

329 By plotting Y' versus $X^{\text{Ap}}_{\text{F}} - X^{\text{Ap}}_{\text{Cl}} - X^{\text{Ap}}_{\text{OH}}$ (Fig. 6b), we can determine the value for

330 $\Delta_r G^{\circ}_{\text{F-Cl}}(2.5\text{GPa}, 800°\text{C})$ to be -19.40±0.76 kJ/mol and a value of -13.06±3.40 kJ/mol for

331 $W^{\text{Ap}}_{\text{F-Cl}}$.

332 By subtracting equation (6.2) from (6.3), we have

333 $$RT\ln(\gamma^{\text{Ap}}_{\text{F}} / \gamma^{\text{Ap}}_{\text{OH}}) = (X^{\text{Ap}}_{\text{OH}} - X^{\text{Ap}}_{\text{F}})W^{\text{Ap}}_{\text{F-OH}} + X^{\text{Ap}}_{\text{Cl}}(W^{\text{Ap}}_{\text{F-Cl}} - W^{\text{Ap}}_{\text{Cl-OH}}) \quad (15)$$

334 Combining equations (5), (8), (11) and (15) gives

335 $$RT\ln K^{\text{Ap-melt}}_{\text{dF-OH}} = -\Delta_r G^{\circ}_{\text{F-OH}}(P,T) + (X^{\text{Ap}}_{\text{F}} - X^{\text{Ap}}_{\text{Cl}} - X^{\text{Ap}}_{\text{OH}})W^{\text{Ap}}_{\text{F-OH}} - X^{\text{Ap}}_{\text{Cl}} \times 10.48\text{kJ/mol} \quad (16)$$

336 For the F-OH exchange equilibrium between apatite and melt, we can perform a

337 similar linear regression based on the following equation

$$Y'' = -\Delta_r G^{\circ}_{\text{F-OH}}(P,T) + (X^{\text{Ap}}_{\text{F}} - X^{\text{Ap}}_{\text{Cl}} - X^{\text{Ap}}_{\text{OH}})W^{\text{Ap}}_{\text{F-OH}} \quad (17)$$

by defining

$$Y'' = RT \ln K_{\text{dF-OH}}^{\text{Ap-melt}} + X^{\text{Ap}}_{\text{Cl}} \times 10.48\text{kJ/mol} \quad (18)$$

The regression results (Fig. 6c) give a value of -53.46±0.68 kJ/mol for $\Delta_r G^{\circ}_{\text{F-OH}}(2.5\text{GPa}, 800°\text{C})$ and a value of -21.32±3.20 kJ/mol for $W^{\text{Ap}}_{\text{F-OH}}$.

4 Discussion

4.1 F and Cl budgets

Based on analytical results for F and Cl content in melt, apatite, phengite and biotite, and the mass fraction of each phase derived from the mass balance of major elements (Table 2), we are able to calculate F and Cl budgets (Fig. 7). Apatite accommodates between 25-60% of the total F, similar to the capacity of melt, while both phengite and biotite contain less than 20% of the total F. In contrast, the majority of the Cl budget resides in melt, with ~70-80% for Cl-OH systems and even higher for F-Cl-OH systems as apatite contains less Cl when F is present. The percentage of bulk Cl accommodated in apatite is ~20% in Cl-OH systems and ≤10% in F-Cl-OH systems. Both phengite and biotite contain less than 5% of the total Cl. Apatite, phengite and biotite always accommodate more F than Cl, whereas melt always contains more Cl than F. This is consistent with amphibole-melt partitioning data showing that F is compatible ($D_{\text{F}}^{\text{Amp-melt}}$ = 1.2-1.9) whereas Cl is incompatible ($D_{\text{Cl}}^{\text{Amp-melt}}$ = 0.08-0.65) for rhyodacitic melt compositions in the *PT* range of 1-3 GPa and 750-1000°C (Van den Bleeken and Koga 2015). In summary, F and Cl budget data suggest that F behaves more compatibly compared to Cl, therefore sediment melting at subduction zone conditions will lead to a

361 decoupling of F and Cl. Fractionation of F and Cl as a result of the dehydration of
362 serpentinite during subduction was also observed by John et al. (2011), that is, an
363 increase of the F/Cl ratio in the residue of the dehydration sequence.

364 While similar F contents are observed in arc and MORB magmas, differences in the
365 origins of F and Cl in arc magmas are highlighted by the far higher Cl content relative to
366 MORB (Van den Bleeken and Koga 2015). Most of the arc melt inclusions reported in
367 the literature have Cl contents between 500 and 2000 ppm (Wallace 2005 and references
368 therein; Portnyagin et al. 2007; Sadofsky et al. 2008 and references therein; Johnson et al.
369 2009), much higher than the Cl content in melt inclusions in Siqueiros transform MORB
370 (1-3 ppm, Saal et al. 2002). Glass and melt inclusions from different arc systems have
371 been reported with F contents in similar ranges, e.g., 250-520 ppm for Kermadec
372 (Wysoczanski et al. 2006) and 99-400 ppm for Kamchatka (Portnyagin et al. 2007). The
373 majority of melt inclusions from the Central America Arc have F contents in the range
374 100-800 ppm (Wade et al. 2006; Sadofsky et al. 2008), with the exception of melt
375 inclusions from Irazu, Costa Rica, containing up to ~3000 ppm F (Benjamin et al. 2007;
376 Sadofsky et al. 2008). The F contents of arc magmas are generally of the same magnitude
377 as those of MORB (e.g., 50-135 ppm, Siqueiros transform, Saal et al. 2002) and OIB
378 (800-1890 ppm, Samoa, Workman et al. 2006; 200-500 ppm, Galápagos, Koleszar et al.
379 2009). This observation is consistent with the previous proposal that F and Cl are
380 effectively fractionated during subduction processes (Jambon 1994; Straub and Layne
381 2003). Straub and Layne (2003) proposed that up to 50% of the F content in the Izu arc
382 front glasses (70-400 ppm) could be juvenile; i.e., it is derived from the sub-arc mantle
383 wedge, while most of the Cl (400-4000 ppm) in the Izu VF melts has its origin in the

subducting slab. Based on their subduction infux and outflux estimates, Straub and Layne (2003) suggested that Cl appears to be almost entirely recycled within arc settings. The fractionation of F and Cl can be further demonstrated by ratios of F/P and Cl/K. As shown by Pyle and Mather (2009), there is a clear increase of Cl/K from MORB (≤ 0.01, Siqueiros transform), to OIB (≤ 0.1, Hawaii, Iceland) to arc magmas (≥ 0.1, Izu, Kamchatka, Central America, Kermadec), while F/P remains broadly constant.

Combined with our experimental results, these data suggest that significant amounts of subducted F can be returned to the deep mantle, and hydrous minerals, in particular apatite, can serve as important carriers of F.

4.2 A comparison of phengite/biotite and apatite partitioning behaviour

The consistency of partition and exchange coefficients for F, Cl and OH exchange between phengite/biotite and melt is in contrast to the variability of such coefficients between apatite and melt. We observed a decrease of $D_{Cl}^{Ap\text{-}melt}$ with increasing F content in apatite/melt. Similar trends also exist for the experimental data of Brenan (1993) and Webster et al. (2009) (see Fig. 11 in Li and Hermann 2015). The exponential decrease of $D_{F}^{Ap\text{-}melt}$ with the increase of F content in apatite/melt mimics the behaviour of F partition coefficients between apatite and aqueous fluid at 0.2 GPa reported by Kusebauch et al. (2015). Therefore, the variations of $D_{Cl}^{Ap\text{-}melt/fluid}$ and $D_{F}^{Ap\text{-}melt/fluid}$ observed in these studies are at least partially caused by the non-ideal mixing of F, Cl and OH in apatite.

A notable similarity between phengite, biotite and apatite is the preferential uptake of F over Cl; such a preference can be attributed to the smaller ionic radius of F compared to Cl that allows easier substitution into the (OH, F, Cl) site. This is also manifested in the

407 relative stability of the F and Cl end-members. A simple comparison of the standard state
408 thermodynamic properties of these end-members sheds some light on the issue. The
409 standard state Gibbs free energies of formation at 25°C and 1 bar for F end-members are
410 smaller than those for Cl end-members for all three phases phengite, biotite and apatite
411 (Zhu and Sverjensky 1992). Moreover, the Gibbs free energies of formation for apatite
412 end-members are lower than those for biotite end-members, which are lower again than
413 values for phengite end-members (Zhu and Sverjensky 1992). This underlies the
414 observation that at equilibrium both F and Cl concentrations decrease in the sequence
415 apatite > biotite > phengite.

416 As we have not assessed the effect of major element composition on F and Cl
417 partitioning in phengite and biotite, namely the reciprocal effect between the octahedral
418 and hydroxyl sites (Zhu and Sverjensky 1992; Icenhower and London 1997), caution is
419 required when applying partition coefficients obtained in this study to phengite and
420 biotite of drastically different compositions. Correlations between $D_F^{Bi\text{-}melt}$, $D_{Cl}^{Bi\text{-}melt}$ and
421 $Mg^{\#}$ in biotite were obtained experimentally at 640 to 680 °C, 0.2 GPa and H_2O saturated
422 conditions by Icenhower and London (1997). For biotites with a $Mg^{\#}$ of 84
423 (100Mg/Mg+Fe in mole%) from this study, the correlations proposed by Icenhower and
424 London (1997) predict $D_F^{Bi\text{-}melt}$ and $D_{Cl}^{Bi\text{-}melt}$ values of ~8 and ~1, respectively.
425 Differences in *P, T* and melt composition notwithstanding, these predicted values are
426 comparable to the observed $D_F^{Bi\text{-}melt}$ (3.7±0.4) and $D_{Cl}^{Bi\text{-}melt}$ (0.86±0.05) values.
427

428 **4.3 Modeling the apatite solid solution at other conditions**

429 In our previous study (Li and Hermann 2015), we also calculated K_ds for F, Cl and OH
430 exchange between apatite and melt for experiments conducted by McCubbin et al. (2015).
431 (2015), Mathez and Webster (2005), Webster et al. (2009) and Doherty et al. (2014).
432 While K_d values showed a general consistency, a certain level of variation was also
433 evident, especially in K_ds for experiments from Webster et al. (2009) and Doherty et al.
434 (2014) (see Fig. 12 of Li and Hermann 2015). The drop in $K_{d\text{Cl-OH}}^{\text{Ap-melt}}$ values with the
435 addition of F to Cl-OH binary apatite, observed in experiments from McCubbin et al.
436 (2015), mimics the observation made for our 2.5 GPa, 800°C experiments. Encouraged
437 by the success of apatite solid solution modeling using our experimental data, we applied
438 the same method to model partitioning data from the above studies. Satisfactory results
439 were obtained from the data of Webster et al. (2009) and Doherty et al. (2014) (Fig. 8;
440 Table 7).

441 A value for $W_{\text{F-OH}}^{\text{Ap}} - W_{\text{F-Cl}}^{\text{Ap}}$ could not be resolved from the regression of
442 $RT \ln K_{d\text{Cl-OH}}^{\text{Ap-melt}}$ versus X_{F}^{Ap} (Fig. 8a) for experiments from Webster et al. (2009), implying
443 the possibility that $W_{\text{F-OH}}^{\text{Ap}} - W_{\text{F-Cl}}^{\text{Ap}} = 0$ at low pressure conditions. Therefore, to account for
444 the variation of $K_{d\text{Cl-OH}}^{\text{Ap-melt}}$ values, we set $W_{\text{Cl-OH}}^{\text{Ap}} \neq 0$, while $W_{\text{F-OH}}^{\text{Ap}} - W_{\text{F-Cl}}^{\text{Ap}} = 0$. By combining
445 these assumptions with equations (3) and (7), we have the following relation:

446 $$RT \ln K_{d\text{Cl-OH}}^{\text{Ap-melt}} = -\Delta_r G_{\text{Cl-OH}}^{\text{o}}(P,T) + (X_{\text{Cl}}^{\text{Ap}} - X_{\text{OH}}^{\text{Ap}}) W_{\text{Cl-OH}}^{\text{Ap}} \quad (19)$$

447 A value of ~17 kJ/mol was derived for $W_{\text{Cl-OH}}^{\text{Ap}}$ from the regression of
448 $RT \ln K_{d\text{Cl-OH}}^{\text{Ap-melt}}$ versus $X_{\text{Cl}}^{\text{Ap}} - X_{\text{OH}}^{\text{Ap}}$ (Fig. 8b).

449 If both $W_{\text{Cl-OH}}^{\text{Ap}}$ and $W_{\text{F-OH}}^{\text{Ap}} - W_{\text{F-Cl}}^{\text{Ap}}$ were set to 0, equations (14) and (17) would be reduced
450 to

$$RT\ln K_{\mathrm{dF\text{-}Cl}}^{\mathrm{Ap\text{-}melt}} = -\Delta_r G_{\mathrm{F\text{-}Cl}}^{\mathrm{o}}(P,T) + (X_{\mathrm{F}}^{\mathrm{Ap}} - X_{\mathrm{Cl}}^{\mathrm{Ap}} - X_{\mathrm{OH}}^{\mathrm{Ap}})W_{\mathrm{F\text{-}Cl}}^{\mathrm{Ap}} \quad (20)$$

$$RT\ln K_{\mathrm{dF\text{-}OH}}^{\mathrm{Ap\text{-}melt}} = -\Delta_r G_{\mathrm{F\text{-}OH}}^{\mathrm{o}}(P,T) + (X_{\mathrm{F}}^{\mathrm{Ap}} - X_{\mathrm{Cl}}^{\mathrm{Ap}} - X_{\mathrm{OH}}^{\mathrm{Ap}})W_{\mathrm{F\text{-}OH}}^{\mathrm{Ap}} \quad (21)$$

respectively. Based on equations (20) and (21), positive values were derived for $W_{\mathrm{F\text{-}Cl}}^{\mathrm{Ap}}$ and $W_{\mathrm{F\text{-}OH}}^{\mathrm{Ap}}$ from regressions of $RT\ln K_{\mathrm{dF\text{-}Cl}}^{\mathrm{Ap\text{-}melt}}$ vs $X_{\mathrm{F}}^{\mathrm{Ap}} - X_{\mathrm{Cl}}^{\mathrm{Ap}} - X_{\mathrm{OH}}^{\mathrm{Ap}}$ and $RT\ln K_{\mathrm{dF\text{-}OH}}^{\mathrm{Ap\text{-}melt}}$ vs $X_{\mathrm{F}}^{\mathrm{Ap}} - X_{\mathrm{Cl}}^{\mathrm{Ap}} - X_{\mathrm{OH}}^{\mathrm{Ap}}$ (Fig. 8c, d).

If we incorporate the positive $W_{\mathrm{Cl\text{-}OH}}^{\mathrm{Ap}}$ value obtained from the regression of $RT\ln K_{\mathrm{dCl\text{-}OH}}^{\mathrm{Ap\text{-}melt}}$ versus $X_{\mathrm{Cl}}^{\mathrm{Ap}} - X_{\mathrm{OH}}^{\mathrm{Ap}}$ (Fig. 8b), we have the following expressions for the regression of $W_{\mathrm{F\text{-}Cl}}^{\mathrm{Ap}}$ and $W_{\mathrm{F\text{-}OH}}^{\mathrm{Ap}}$:

$$RT\ln K_{\mathrm{dF\text{-}Cl}}^{\mathrm{Ap\text{-}melt}} - X_{\mathrm{OH}}^{\mathrm{Ap}} \times W_{\mathrm{Cl\text{-}OH}}^{\mathrm{Ap}} = -\Delta_r G_{\mathrm{F\text{-}Cl}}^{\mathrm{o}}(P,T) + (X_{\mathrm{F}}^{\mathrm{Ap}} - X_{\mathrm{Cl}}^{\mathrm{Ap}} - X_{\mathrm{OH}}^{\mathrm{Ap}})W_{\mathrm{F\text{-}Cl}}^{\mathrm{Ap}} \quad (22.1)$$

$$RT\ln K_{\mathrm{dF\text{-}OH}}^{\mathrm{Ap\text{-}melt}} - X_{\mathrm{Cl}}^{\mathrm{Ap}} \times W_{\mathrm{Cl\text{-}OH}}^{\mathrm{Ap}} = -\Delta_r G_{\mathrm{F\text{-}OH}}^{\mathrm{o}}(P,T) + (X_{\mathrm{F}}^{\mathrm{Ap}} - X_{\mathrm{Cl}}^{\mathrm{Ap}} - X_{\mathrm{OH}}^{\mathrm{Ap}})W_{\mathrm{F\text{-}OH}}^{\mathrm{Ap}} \quad (22.2)$$

The resultant $W_{\mathrm{F\text{-}Cl}}^{\mathrm{Ap}}$ and $W_{\mathrm{F\text{-}OH}}^{\mathrm{Ap}}$ values are higher than those derived from the previous approach, but with the same sign and magnitude (Fig. 8e, f).

Neither $W_{\mathrm{F\text{-}OH}}^{\mathrm{Ap}} - W_{\mathrm{F\text{-}Cl}}^{\mathrm{Ap}}$ nor $W_{\mathrm{Cl\text{-}OH}}^{\mathrm{Ap}}$ can be resolved from the regression of $RT\ln K_{\mathrm{dCl\text{-}OH}}^{\mathrm{Ap\text{-}melt}}$ versus $X_{\mathrm{F}}^{\mathrm{Ap}}$ and $X_{\mathrm{Cl}}^{\mathrm{Ap}} - X_{\mathrm{OH}}^{\mathrm{Ap}}$ respectively for experiments from Doherty et al. (2014). Note that it is not plausible to perform multi-variable regression with both $X_{\mathrm{F}}^{\mathrm{Ap}}$ and $X_{\mathrm{Cl}}^{\mathrm{Ap}} - X_{\mathrm{OH}}^{\mathrm{Ap}}$ as independent variables due to the fact that they are correlated. The regressions of $K_{\mathrm{dF\text{-}Cl}}^{\mathrm{Ap\text{-}melt}}$ and $K_{\mathrm{dF\text{-}OH}}^{\mathrm{Ap\text{-}melt}}$ data were performed based on equations (20) and (21) (Fig. 8g, h). The obtained values for $W_{\mathrm{F\text{-}Cl}}^{\mathrm{Ap}}$ and $W_{\mathrm{F\text{-}OH}}^{\mathrm{Ap}}$ show good agreement with the regression results for experiments from Webster et al. (2009).

4.4 Calculating melt Cl and F contents based on apatite composition

F, Cl and OH exchange coefficients between apatite and melt (K_d) can be used to derive information regarding the F, Cl and OH contents in melt based on apatite compositions. Using $K_{d\text{Cl-OH}}^{\text{Ap-melt}}$ as an example, we can derive the following relation from the definition for $K_{d\text{Cl-OH}}^{\text{Ap-melt}}$ in equation (2),

$$\frac{X_{\text{Cl}}^{\text{melt}}}{X_{\text{OH}}^{\text{melt}}} = \frac{X_{\text{Cl}}^{\text{Ap}}}{X_{\text{OH}}^{\text{Ap}}} \times \frac{1}{K_{d\text{Cl-OH}}^{\text{Ap-melt}}} \quad (23)$$

Furthermore, by plotting the melt Cl content (wt%) versus the molar ratio $X_{\text{Cl}}^{\text{melt}} / X_{\text{OH}}^{\text{melt}}$ for the EPSM-1, 2 and 5 experiments reported in Li and Hermann (2015) covering the *PT* range 2.5-4.5 GPa and 690-900°C, we are able to obtain the following empirical linear relationship between these two variables (Fig. 9a), given by the equation:

$$C_{\text{Cl}}^{\text{melt}} = (X_{\text{Cl}}^{\text{melt}} / X_{\text{OH}}^{\text{melt}}) \times 28.72(\pm 1.04) \quad (24)$$

Combining equations (23), (24) and the $K_{d\text{Cl-OH}}^{\text{Ap-melt}}$ values obtained in Li and Hermann (2015) enable estimation of melt Cl content based on apatite composition in the *PT* range 2.5-4.5 GPa and 690-900°C. Similar relations as in equation (24) also exist for experiments from McCubbin et al. (2015) and Webster et al. (2009) (Fig. 9), with expressions

$$C_{\text{Cl}}^{\text{melt}} = (X_{\text{Cl}}^{\text{melt}} / X_{\text{OH}}^{\text{melt}}) \times 9.12(\pm 0.11) \quad (25)$$

for experiments from McCubbin et al. (2015);

$$C_{\text{Cl}}^{\text{melt}} = (X_{\text{Cl}}^{\text{melt}} / X_{\text{OH}}^{\text{melt}}) \times 10.79(\pm 0.52) \quad (26.1)$$

$$\text{and } C_{\text{F}}^{\text{melt}} = (X_{\text{F}}^{\text{melt}} / X_{\text{OH}}^{\text{melt}}) \times 6.18(\pm 0.41) \quad (26.2)$$

for experiments from Webster et al. (2009).

The applicability of equations (24)-(26) should not be affected by the uncertainties associated with the calculation of $X_{\mathrm{OH}}^{\mathrm{melt}}$, as the derivation of $K_{\mathrm{dCl\text{-}OH}}^{\mathrm{Ap\text{-}melt}}$ and the relations in equations (24)-(26) are based on the same $X_{\mathrm{OH}}^{\mathrm{melt}}$ data, and are thus considered to be internally consistent.

When K_{d}s show variation as a function of apatite composition, their values can be determined based on the thermodynamic expressions for F, Cl and OH exchange between apatite and melt, and the regression results for $-\Delta_r G^{\mathrm{o}}_{\mathrm{Cl\text{-}OH}}(P,T)$, $-\Delta_r G^{\mathrm{o}}_{\mathrm{F\text{-}OH}}(P,T)$, $-\Delta_r G^{\mathrm{o}}_{\mathrm{F\text{-}Cl}}(P,T)$, $W^{\mathrm{Ap}}_{\mathrm{Cl\text{-}OH}}$, $W^{\mathrm{Ap}}_{\mathrm{F\text{-}Cl}}$ and $W^{\mathrm{Ap}}_{\mathrm{F\text{-}OH}}$. For example, $K_{\mathrm{dCl\text{-}OH}}^{\mathrm{Ap\text{-}melt}}$ values can be obtained based on the relations in equation (3) and (7), with the following equation:

$$K_{\mathrm{dCl\text{-}OH}}^{\mathrm{Ap\text{-}melt}} = \mathrm{EXP}\left\{\left[-\Delta_r G^{\mathrm{o}}_{\mathrm{Cl\text{-}OH}}(P,T) + (X^{\mathrm{Ap}}_{\mathrm{Cl}} - X^{\mathrm{Ap}}_{\mathrm{OH}})W^{\mathrm{Ap}}_{\mathrm{Cl\text{-}OH}} + X^{\mathrm{Ap}}_{\mathrm{F}}(W^{\mathrm{Ap}}_{\mathrm{F\text{-}OH}} - W^{\mathrm{Ap}}_{\mathrm{F\text{-}Cl}})\right]\times 10^3 / 8.314 / T\right\} \quad (27)$$

where the units for $-\Delta_r G^{\mathrm{o}}_{\mathrm{Cl\text{-}OH}}(P,T)$ and Ws are kJ/mol, and T is in Kelvin. Similar equation can be derived for $K_{\mathrm{dF\text{-}OH}}^{\mathrm{Ap\text{-}melt}}$ based on the relations in equation (5) and (15):

$$K_{\mathrm{dF\text{-}OH}}^{\mathrm{Ap\text{-}melt}} = \mathrm{EXP}\left\{\left[-\Delta_r G^{\mathrm{o}}_{\mathrm{F\text{-}OH}}(P,T) + (X^{\mathrm{Ap}}_{\mathrm{F}} - X^{\mathrm{Ap}}_{\mathrm{OH}})W^{\mathrm{Ap}}_{\mathrm{F\text{-}OH}} + X^{\mathrm{Ap}}_{\mathrm{Cl}}(W^{\mathrm{Ap}}_{\mathrm{Cl\text{-}OH}} - W^{\mathrm{Ap}}_{\mathrm{F\text{-}Cl}})\right]\times 10^3 / 8.314 / T\right\} \quad (28)$$

Equations (26), (27) and (28) have been used to estimate the Cl and F contents in felsic melts at 0.2 GPa, 800°C based on the natural apatite compositions listed in Table 3 of Webster et al. (2009). The values used in the calculations are 25.81±1.05 kJ/mol for $-\Delta_r G^{\mathrm{o}}_{\mathrm{Cl\text{-}OH}}(P,T)$, 40.33±1.21 kJ/mol for $-\Delta_r G^{\mathrm{o}}_{\mathrm{F\text{-}OH}}(P,T)$, 17.33±6.22 kJ/mol for $W^{\mathrm{Ap}}_{\mathrm{Cl\text{-}OH}}$ and $W^{\mathrm{Ap}}_{\mathrm{F\text{-}OH}} = W^{\mathrm{Ap}}_{\mathrm{F\text{-}Cl}}$=21.29±2.96 kJ/mol. The resultant Cl and F contents in melts are listed in Table 8 along with the reported apatite compositions and calculated $K_{\mathrm{dCl\text{-}OH}}^{\mathrm{Ap\text{-}melt}}$ and $K_{\mathrm{dF\text{-}OH}}^{\mathrm{Ap\text{-}melt}}$ values. The calculated melt Cl contents show excellent agreement with the estimations made by Webster et al. (2009) based on Cl partitioning data (Fig. 10). The

514 calculated F contents in melt are also similar to the estimation made by Webster et al.
515 (2009) based on F partitioning data, but with larger relative error (Table 8).
516
517 **4.5 Implications for the thermodynamic properties of apatite**
518 We have successfully derived Margules parameters for F, Cl and OH mixing in apatite
519 based on F, Cl and OH partitioning data at 2.5 GPa, 800°C and 0.2 GPa, 0.05 GPa,
520 ~900°C (Webster et al. 2009; Doherty et al. 2014). In clear contrast, positive values were
521 obtained for $W_{\text{Cl-OH}}^{\text{Ap}}$, $W_{\text{F-Cl}}^{\text{Ap}}$ and $W_{\text{F-OH}}^{\text{Ap}}$ at 0.2 GPa, 0.05 GPa, 900°C, while zero to negative
522 values were obtained at 2.5 GPa, 800°C. Variation in K_{d} values is relatively small for 1
523 GPa, ~1000°C experiments from McCubbin et al. (2015) and 0.2 GPa, ~1100°C
524 experiments from Mathez and Webster (2005), indicating that non-ideal mixing in the
525 apatite solid solution has negligible effect on K_{d} values at these high temperature
526 conditions within the compositional range of X_{F}^{Ap}>0.2 (McCubbin et al. 2015).
527 Modeling hydrous silicate melts as ideal mixtures of H_2O molecules (H_2O_m), OH, O,
528 Cl and F significantly simplifies the description of F, Cl and OH exchange between
529 apatite and melt. As both F and Cl constitute trace elements in melt, an ideal mixing
530 model should be sufficient. The H_2O content of melts in each data set remains nearly
531 constant for the given *PT* conditions, as does the mole fraction of OH, a major H_2O
532 species in melt. As a result, the $X_{\text{OH}}^{\text{melt}}$ term cancels out in linear regressions performed to
533 derive Margules parameters. Using the regression based on equation (9) as an example,
534 the slope of the linear regression can be formulated as the change in *y* divided by the
535 change in *x* between two data points *a* and *b*, i.e.,
536
$$W_{\text{F-OH}}^{\text{Ap}} - W_{\text{F-Cl}}^{\text{Ap}} = \Delta(RT \ln K_{\text{dCl-OH}}^{\text{Ap-melt}})_{a-b} / \Delta(X_{\text{F}}^{\text{Ap}})_{a-b} \quad (29)$$

537 Based on the definition for $K_{\mathrm{d}\,\mathrm{Cl\text{-}OH}}^{\mathrm{Ap\text{-}melt}}$ in equation (2), we have

538 $$\Delta(RT\ln K_{\mathrm{dCl\text{-}OH}}^{\mathrm{Ap\text{-}melt}})_{a-b} = RT\ln\left[\frac{(X_{\mathrm{Cl}}^{\mathrm{Ap}})_a\times(X_{\mathrm{OH}}^{\mathrm{melt}})_a}{(X_{\mathrm{OH}}^{\mathrm{Ap}})_a\times(X_{\mathrm{Cl}}^{\mathrm{melt}})_a}\Big/\frac{(X_{\mathrm{Cl}}^{\mathrm{Ap}})_b\times(X_{\mathrm{OH}}^{\mathrm{melt}})_b}{(X_{\mathrm{OH}}^{\mathrm{Ap}})_b\times(X_{\mathrm{Cl}}^{\mathrm{melt}})_b}\right] \quad (30)$$

539 $$\text{As } (X_{\mathrm{OH}}^{\mathrm{melt}})_a = (X_{\mathrm{OH}}^{\mathrm{melt}})_b \ , \quad (31)$$

540 equation (30) is reduced to

541 $$\Delta(RT\ln K_{\mathrm{dCl\text{-}OH}}^{\mathrm{Ap\text{-}melt}})_{a-b} = RT\ln\left[\frac{(X_{\mathrm{Cl}}^{\mathrm{Ap}})_a}{(X_{\mathrm{OH}}^{\mathrm{Ap}})_a\times(X_{\mathrm{Cl}}^{\mathrm{melt}})_a}\Big/\frac{(X_{\mathrm{Cl}}^{\mathrm{Ap}})_b}{(X_{\mathrm{OH}}^{\mathrm{Ap}})_b\times(X_{\mathrm{Cl}}^{\mathrm{melt}})_b}\right] \ , \quad (32)$$

542 which indicates that the slope of the linear regression $W_{\mathrm{F\text{-}OH}}^{\mathrm{Ap}} - W_{\mathrm{F\text{-}Cl}}^{\mathrm{Ap}}$ is independent of the
543 calculations for $X_{\mathrm{OH}}^{\mathrm{melt}}$. Therefore, the method used to calculate $X_{\mathrm{OH}}^{\mathrm{melt}}$ only affects the
544 absolute values of $K_{\mathrm{dCl\text{-}OH}}^{\mathrm{Ap\text{-}melt}}$ and $K_{\mathrm{dF\text{-}OH}}^{\mathrm{Ap\text{-}melt}}$, and consequently the values of $-\Delta_r G_{\mathrm{Cl\text{-}OH}}^{\mathrm{o}}(P,T)$
545 and $-\Delta_r G_{\mathrm{F\text{-}OH}}^{\mathrm{o}}(P,T)$, but has negligible effect on the values of Margules parameters. In
546 both this and our previous study (Li and Hermann 2015), the equilibrium constant K_1 for
547 the reaction H_2O_m (melt) + O (melt) = 2OH (melt), at 2.5-4.5 GPa, was calculated based
548 on the ideal-mixing of H_2O species in rhyolitic melt at 2.83 GPa from Hui et al. (2008).
549 The resultant K_1 ranges from 0.27 to 0.41 in accordance with the temperature range 963-
550 1173 K. As reported by Hui et al. (2008), the effect of pressure on K_1 is much smaller
551 than the effect of temperature; a change caused by 1.9 GPa pressure increase (from 0.94
552 to 2.83 GPa) at 873 K is equivalent to a temperature effect of 49 K (from 873 K to 922 K)
553 at 0.94 GPa. When increasing pressure from 2.5 to 4.5 GPa, the difference in K_1 is equal
554 to a temperature increase of 50 K at 2.83 GPa, that is, a small increase of 0.04. What
555 remains unanswered is what effect high H_2O content in melt (10-40 wt%) may have on
556 K_1. However, by testing our data with variable K_1 values, we observed that the difference
557 in calculated X_{OH} in melt in response to a variation of up to 0.2 for K_1, is within the

558 uncertainty of the H_2O content in melt. Therefore we consider the adopted K_1 values
559 reasonable for the intended purpose. Moreover, $K_{dF\text{-}Cl}^{Ap\text{-}melt}$ values are independent of the
560 determination of mole fractions of H_2O species in melt. The excellent agreement between
561 the regression of $K_{dF\text{-}Cl}^{Ap\text{-}melt}$ and $K_{dF\text{-}OH}^{Ap\text{-}melt}$ data demonstrates the success of the chosen
562 hydrous melt model. The success of such regression also suggests that the choice of a
563 regular solution model for apatite was also reasonable. An asymmetric model would
564 require extra Margules parameters, introducing an excess of variables and rendering the
565 regression unresolvable for the limited data sets available.

566 There have been previous attempts to make direct measurements of thermodynamic
567 properties for apatite solid solutions (Dachs et al. 2010; Hovis and Harlov 2010; Hovis et
568 al. 2014a, 2014b, 2015); however, the interpretation of such data remains difficult and
569 uncertain. Hovis and Harlov (2010) and Hovis et al. (2014a) measured the enthalpies of
570 F-Cl and F-OH mixing, as the difference between the solution calorimetric measurements
571 of the apatite binary solution and the line of ideal mixing. Although the average standard
572 deviation of the solution calorimetric measurement was reasonably small (1.1 kJ/mol,
573 Hovis and Harlov 2010), the enthalpy of mixing represents the difference between two
574 large numbers of similar value, and the determination was hampered by evident data
575 scattering (Hovis and Harlov 2010). A detrimental issue associated with this process is
576 the uncertainty in determining the line of ideal mixing, where different choices of apatite
577 end-members may result in either positive or negative values for the enthalpy of mixing
578 (Hovis and Harlov 2010; Hovis et al. 2014a).

579 Values for $W_{Cl\text{-}OH}^{Ap}$, $W_{F\text{-}Cl}^{Ap}$ and $W_{F\text{-}OH}^{Ap}$ at 0.2 GPa, 0.05 GPa, 900°C fall in the range ~15 to
580 ~25 kJ/mol, implying immiscibility for Cl-OH, F-Cl and F-OH apatite binary solid

581 solutions. However, the general consensus is that complete solubility occurs between F,
582 Cl and OH in apatite (e.g., Pan and Fleet 2002). Further investigation is required to
583 reconcile these observations. It is possible that the stabilizing effect of impurities, e.g.,
584 vacancies and oxygens in the c-axis anion channel, contributes to the extended miscibility
585 of apatite solutions.

586 As stated in the review of apatite sensu stricto structure by Hughes and Rakovan
587 (2002), the Ca2 cations (from CaO_6(F,OH) polyhedra) form triangles on the planes at
588 z=1/4 and z=3/4. F, the smallest of the three anions, lies on the plane at z=1/4, 3/4. The
589 larger OH anionic complex and the Cl anion are too large to lie on the rigid plane defined
590 by the Ca atoms, and OH and Cl anions are displaced above or below the plane. The
591 structural configurations of apatite end-members are not miscible without a structural
592 response to the mixing of F, Cl and OH (Hughes and Rakovan 2002), which suggests the
593 likelihood of non-ideal mixing of F, Cl and OH in apatite. For example, Cl could not
594 coexist with other anions in the columns without structural adjustment. When
595 accommodating an OH neighbor, a new Cl position is created which is closer to the z=3/4
596 mirror plane (Sudarsanan and Young 1978; Hughes et al. 1990). The structural response
597 of apatite to F, Cl and OH mixing is certainly a complex issue (Hughes and Rakovan
598 2015). Further investigation of this matter will doubtlessly help elucidate the
599 thermodynamic properties of F, Cl and OH mixing in the apatite solid solution.
600

601 **5 Implications**

602 The Nernstian partitioning of Cl and F between phengite/biotite and melt suggests ideal
603 mixing of F, Cl and OH in phengite, biotite and melt. Thus, biotite and phengite can be

604 useful monitors for halogen contents in hydrous silicate melts. The disadvantage of these
605 phases is that F and Cl concentrations may be too low to detect with electron-beam
606 techniques and would require analysis by Ion probe. Our study has shown that apatite has
607 significantly higher Cl and F contents than biotite and phengite. However, non-ideal
608 mixing in apatite is responsible for the non-Nernstian partitioning between apatite and
609 melt. Exchange coefficients for F, Cl and OH partitioning between apatite and melt (K_d)
610 are better suited parameters for deriving information regarding F, Cl and OH contents in
611 melt. The ternary solution model for apatite developed in this study enables calculation of
612 K_ds based on the thermodynamic expressions for F, Cl and OH exchange reactions
613 between apatite and melt. Direct measurements of thermodynamic properties for apatite
614 solid solutions are scarce (Hovis and Harlov 2010; Hovis et al. 2014a, 2014b, 2015).
615 Ongoing research in this area will help to evaluate apatite solid solution models obtained
616 from phase equilibrium studies and enhance the utility of apatite as a sensor of halogen
617 concentrations in hydrous silicate melts.
618

619 **Acknowledgement**

620 We would like to thank D. Clark and D. Scott for their assistance with the experimental
621 program, and F. Brink and R. Rapp for their help with SEM and electron microprobe
622 analyses. Constructive reviews from Gokce Ustunisik and Guy Hovis were appreciated.
623 This project was financially supported by the Australian Research Council.
624

625 **References:**

626 Barnes, J.J., Franchi, I.A., Anand, M., Tartèse, R., Starkey, N.A., Koike, M., Sano, Y.,

627 and Russell, S.S. (2013) Accurate and precise measurements of the D/H ratio and
628 hydroxyl content in lunar apatites using NanoSIMS. Chemical Geology, 337-338,
629 48–55.
630 Barnes, J.J., Tartèse, R., Anand, M., McCubbin, F.M., Franchi, I. a., Starkey, N. a., and
631 Russell, S.S. (2014) The origin of water in the primitive Moon as revealed by the
632 lunar highlands samples. Earth and Planetary Science Letters, 390, 244–252.
633 Benjamin, E.R., Plank, T., Wade, J. a., Kelley, K. a., Hauri, E.H., and Alvarado, G.E.
634 (2007) High water contents in basaltic magmas from Irazú Volcano, Costa Rica.
635 Journal of Volcanology and Geothermal Research, 168, 68–92.
636 Boudreau, A.E., and McCallum, I.S. (1989) Investigations of the Stillwater Complex:
637 Part V. Apatites as indicators of evolving fluid composition. Contributions to
638 Mineralogy and Petrology, 102, 138–153.
639 Boyce, J.W., and Hervig, R.L. (2008) Magmatic degassing histories from apatite volatile
640 stratigraphy. Geology, 36, 63.
641 Boyce, J.W., Liu, Y., Rossman, G.R., Guan, Y., Eiler, J.M., Stolper, E.M., and Taylor, L.
642 a (2010) Lunar apatite with terrestrial volatile abundances. Nature, 466, 466–469.
643 Boyce, J.W., Tomlinson, S.M., McCubbin, F.M., Greenwood, J.P., and Treiman, A.H.
644 (2014) The Lunar Apatite Paradox. Science, 344, 400–402.
645 Brenan, J.M. (1993) Partitioning of fluorine and chlorine between apatite and aqueous
646 fluids at high pressure and temperature: implications for the F and Cl content of
647 highP-T fluids. Earth and Planetary Science Letters, 117, 251–263.
648 Dachs, E., Harlov, D., and Benisek, A. (2010) Excess heat capacity and entropy of
649 mixing along the chlorapatite–fluorapatite binary join. Physics and Chemistry of

650 Minerals, 37, 665–676.
651 Doherty, A.L., Webster, J.D., Goldoff, B. a., and Piccoli, P.M. (2014) Partitioning
652 behavior of chlorine and fluorine in felsic melt–fluid(s)–apatite systems at 50MPa
653 and 850–950°C. Chemical Geology, 384, 94–111.
654 Greenwood, J.P., Itoh, S., Sakamoto, N., Warren, P., Taylor, L., and Yurimoto, H. (2011)
655 Hydrogen isotope ratios in lunar rocks indicate delivery of cometary water to the
656 Moon. Nature Geoscience, 4, 79–82.
657 Gross, J., Filiberto, J., and Bell, A.S. (2013) Water in the martian interior: Evidence for
658 terrestrial MORB mantle-like volatile contents from hydroxyl-rich apatite in
659 olivine–phyric shergottite NWA 6234. Earth and Planetary Science Letters, 369-370,
660 120–128.
661 Harlov, D., Renzulli, A., and Ridolfi, F. (2006) Iron-bearing chlor-fluorapatites in crustal
662 xenoliths from the Stromboli volcano (Aeolian Islands, Southern Italy): an indicator
663 of fluid processes during contact metamorphism. Eur. J. Mineral., 18, 233.
664 Hovis, G., Abraham, T., Hudacek, W., Wildermuth, S., Scott, B., Altomare, C., Medford,
665 A., Conlon, M., Morris, M., Leaman, A., and others (2015) Thermal expansion of F-
666 Cl apatite crystalline solutions. American Mineralogist, 100, 1040–1046.
667 Hovis, G.L., and Harlov, D.E. (2010) Solution calorimetric investigation of fluor-
668 chlorapatite crystalline solutions. American Mineralogist, 95, 946–952.
669 Hovis, G.L., McCubbin, F.M., Nekvasil, H., Ustunisik, G., Woerner, W.R., and Lindsley,
670 D.H. (2014a) A novel technique for fluorapatite synthesis and the thermodynamic
671 mixing behavior of F-OH apatite crystalline solutions. American Mineralogist, 99,
672 890–897.

673 Hovis, G.L., Scott, B.T., Altomare, C.M., Leaman, A.R., Morris, M.D., Tomaino, G.P.,
674 and McCubbin, F.M. (2014b) Thermal expansion of fluorapatite-hydroxylapatite
675 crystalline solutions. American Mineralogist, 99, 2171–2175.
676 Howarth, G.H., Pernet-Fisher, J.F., Bodnar, R.J., and Taylor, L.A. (2015) Evidence for
677 the exsolution of Cl-rich fluids in martian magmas: Apatite petrogenesis in the
678 enriched lherzolitic shergottite Northwest Africa 7755. Geochimica et
679 Cosmochimica Acta, 166, 234–248.
680 Hughes, J.M., and Rakovan, J. (2002) The Crystal Structure of Apatite,
681 Ca5(PO4)3(F,OH,Cl). Reviews in Mineralogy and Geochemistry, 48, 1–12.
682 Hughes, J.M., and Rakovan, J.F. (2015) Structurally Robust, Chemically Diverse: Apatite
683 and Apatite Supergroup Minerals. Elements, 11, 165–170.
684 Hughes, J.M., Cameron, M., and Crowley, K.D. (1990) Crystal structures of natural
685 ternary apatites; solid solution in the Ca5(PO4)3 X(X = F, OH, Cl) system.
686 American Mineralogist, 75, 295–304.
687 Hui, H., Zhang, Y., Xu, Z., and Behrens, H. (2008) Pressure dependence of the speciation
688 of dissolved water in rhyolitic melts. Geochimica et Cosmochimica Acta, 72, 3229–
689 3240.
690 Icenhower, J.P., and London, D. (1997) Partitioning of fluorine and chlorine between
691 biotite and granitic melt: experimental calibration at 200 MPa H 2 O. Contributions
692 to Mineralogy and Petrology, 127, 17–29.
693 Jambon, A. (1994) Earth degassing and large-scale geochemical cycling of volatile
694 elements. Reviews in Mineralogy and Geochemistry, 30, 479–517.
695 John, T., Scambelluri, M., Frische, M., Barnes, J.D., and Bach, W. (2011) Dehydration of

696 subducting serpentinite: Implications for halogen mobility in subduction zones and
697 the deep halogen cycle. Earth and Planetary Science Letters, 308, 65–76.
698 Johnson, E.R., Wallace, P.J., Delgado Granados, H., Manea, V.C., Kent, A.J.R.,
699 Bindeman, I.N., and Donegan, C.S. (2009) Subduction-related Volatile Recycling
700 and Magma Generation beneath Central Mexico: Insights from Melt Inclusions,
701 Oxygen Isotopes and Geodynamic Models. Journal of Petrology, 50, 1729–1764.
702 Jones, R.H., McCubbin, F.M., Dreeland, L., Guan, Y., Burger, P. V., and Shearer, C.K.
703 (2014) Phosphate minerals in LL chondrites: A record of the action of fluids during
704 metamorphism on ordinary chondrite parent bodies. Geochimica et Cosmochimica
705 Acta, 132, 120–140.
706 Khorzhinskiy, M.A. (1981) Apatite solid solutions as indicators of the fugacity of HCl
707 and HF in hydrothermal fluids. Geochemistry International, 18, 44–60.
708 Koleszar, A.M., Saal, A.E., Hauri, E.H., Nagle, A.N., Liang, Y., and Kurz, M.D. (2009)
709 The volatile contents of the Galapagos plume; evidence for H2O and F open system
710 behavior in melt inclusions. Earth and Planetary Science Letters, 287, 442–452.
711 Kusebauch, C., John, T., Whitehouse, M.J., Klemme, S., and Putnis, A. (2015)
712 Distribution of halogens between fluid and apatite during fluid-mediated
713 replacement processes. Geochimica et Cosmochimica Acta, 170, 225–246.
714 Li, H., and Hermann, J. (2015) Apatite as an indicator of fluid salinity: An experimental
715 study of chlorine and fluorine partitioning in subducted sediments. Geochimica et
716 Cosmochimica Acta, 166, 267–297.
717 Mathez, E.A., and Webster, J.D. (2005) Partitioning behavior of chlorine and fluorine in
718 the system apatite-silicate melt-fluid. Geochimica et Cosmochimica Acta, 69, 1275–

719 1286.

720 McCubbin, F.M., Steele, A., Nekvasil, H., Schnieders, A., Rose, T., Fries, M., Carpenter,
721 P.K., and Jolliff, B.L. (2010a) Detection of structurally bound hydroxyl in
722 fluorapatite from Apollo Mare basalt 15058,128 using TOF-SIMS. American
723 Mineralogist, 95, 1141–1150.

724 McCubbin, F.M., Steele, A., Hauri, E.H., Nekvasil, H., Yamashita, S., and Hemley, R.J.
725 (2010b) Nominally hydrous magmatism on the Moon. Proceedings of the National
726 Academy of Sciences, 107, 11223–11228.

727 McCubbin, F.M., Hauri, E.H., Elardo, S.M., Vander Kaaden, K.E., Wang, J., and Shearer,
728 C.K. (2012) Hydrous melting of the martian mantle produced both depleted and
729 enriched shergottites. Geology, 40, 683–686.

730 McCubbin, F.M., Vander Kaaden, K.E., Tartèse, R., Boyce, J.W., Mikhail, S., Whitson,
731 E.S., Bell, A.S., Anand, M., Franchi, I.A., Wang, J., and others (2015) Experimental
732 investigation of F, Cl, and OH partitioning between apatite and Fe-rich basaltic melt
733 at 1.0–1.2 GPa and 950–1000 °C. American Mineralogist, 100, 1790–1802.

734 O'Reilly, S.Y., and Griffin, W.. (2000) Apatite in the mantle: implications for
735 metasomatic processes and high heat production in Phanerozoic mantle. Lithos, 53,
736 217–232.

737 Pan, Y., and Fleet, M.E. (2002) Compositions of the Apatite-Group Minerals:
738 Substitution Mechanisms and Controlling Factors. Reviews in Mineralogy and
739 Geochemistry, 48, 13–49.

740 Patiño Douce, A.E., and Roden, M. (2006) Apatite as a probe of halogen and water
741 fugacities in the terrestrial planets. Geochimica et Cosmochimica Acta, 70, 3173–

3196.

Patiño Douce, A.E., Roden, M.F., Chaumba, J., Fleisher, C., and Yogodzinski, G. (2011) Compositional variability of terrestrial mantle apatites, thermodynamic modeling of apatite volatile contents, and the halogen and water budgets of planetary mantles. Chemical Geology, 288, 14–31.

Piccoli, P., and Candela, P. (1994) Apatite in felsic rocks; a model for the estimation of initial halogen concentrations in the Bishop Tuff (Long Valley) and Tuolumne Intrusive Suite (Sierra Nevada Batholith) magmas. American Journal of Science, 294, 92–135.

Piccoli, P.M., and Candela, P.A. (2002) Apatite in Igneous Systems. Reviews in Mineralogy and Geochemistry, 48, 255–292.

Plank, T., and Langmuir, C.H. (1998) The chemical composition of subducting sediment and its consequences for the crust and mantle. Chemical Geology, 145, 325–394.

Portnyagin, M., Hoernle, K., Plechov, P., Mironov, N., and Khubunaya, S. (2007) Constraints on mantle melting and composition and nature of slab components in volcanic arcs from volatiles (H2O, S, Cl, F) and trace elements in melt inclusions from the Kamchatka Arc. Earth and Planetary Science Letters, 255, 53–69.

Pyle, D.M., and Mather, T.A. (2009) Halogens in igneous processes and their fluxes to the atmosphere and oceans from volcanic activity: A review. Chemical Geology, 263, 110–121.

Rudnick, R.L., and Gao, S. (2003) Composition of the Continental Crust. In Treatise on Geochemistry Vol. 1, pp. 1–64. Elsevier.

Saal, A.E., Hauri, E.H., Langmuir, C.H., and Perfit, M.R. (2002) Vapour undersaturation

765 in primitive mid-ocean-ridge basalt and the volatile content of Earth's upper mantle.
766 Nature, 419, 451–455.
767 Sadofsky, S.J., Portnyagin, M., Hoernle, K., and van den Bogaard, P. (2008) Subduction
768 cycling of volatiles and trace elements through the Central American volcanic arc:
769 evidence from melt inclusions. Contributions to Mineralogy and Petrology, 155,
770 433–456.
771 Scambelluri, M., Müntener, O., Ottolini, L., Pettke, T.T., and Vannucci, R. (2004) The
772 fate of B, Cl and Li in the subducted oceanic mantle and in the antigorite breakdown
773 fluids. Earth and Planetary Science Letters, 222, 217–234.
774 Silver, L., and Stolper, E. (1985) A Thermodynamic Model for Hydrous Silicate Melts.
775 The Journal of Geology, 93, 161–177.
776 Spear, F.S., and Pyle, J.M. (2002) Apatite, Monazite, and Xenotime in Metamorphic
777 Rocks. Reviews in Mineralogy and Geochemistry, 48, 293–335.
778 Straub, S.M., and Layne, G.D. (2003) The systematics of chlorine, fluorine, and water in
779 Izu arc front volcanic rocks: Implications for volatile recycling in subduction zones.
780 Geochimica et Cosmochimica Acta, 67, 4179–4203.
781 Sudarsanan, K., and Young, R.A. (1978) Structural interactions of F, Cl and OH in
782 apatites. Acta Crystallographica Section B Structural Crystallography and Crystal
783 Chemistry, 34, 1401–1407.
784 Tartèse, R., Anand, M., Barnes, J.J., Starkey, N. a., Franchi, I. a., and Sano, Y. (2013)
785 The abundance, distribution, and isotopic composition of Hydrogen in the Moon as
786 revealed by basaltic lunar samples: Implications for the volatile inventory of the
787 Moon. Geochimica et Cosmochimica Acta, 122, 58–74.

788 Tartèse, R., Anand, M., McCubbin, F.M., Elardo, S.M., Shearer, C.K., and Franchi, I. a.
789 (2014) Apatites in lunar KREEP basalts: The missing link to understanding the H
790 isotope systematics of the Moon. Geology, 42, 363–366.
791 Taylor, S.R., and McLennan, S.M. (1985) The Continental Crust: its Composition and
792 Evolution. Oxford: Blackwell.
793 Van den Bleeken, G., and Koga, K.T. (2015) Experimentally determined distribution of
794 fluorine and chlorine upon hydrous slab melting, and implications for F-Cl cycling
795 through subduction zones. Geochimica et Cosmochimica Acta, 171, 353–373.
796 Wade, J.A., Plank, T., Melson, W.G., Soto, G.J., and Hauri, E.H. (2006) The volatile
797 content of magmas from Arenal volcano, Costa Rica. Journal of Volcanology and
798 Geothermal Research, 157, 94–120.
799 Wallace, P.J. (2005) Volatiles in subduction zone magmas: concentrations and fluxes
800 based on melt inclusion and volcanic gas data. Journal of Volcanology and
801 Geothermal Research, 140, 217–240.
802 Webster, J.D., and De Vivo, B. (2002) Experimental and modeled solubilities of chlorine
803 in aluminosilicate melts, consequences of magma evolution, and implications for
804 exsolution of hydrous chloride melt at Mt. Somma-Vesuvius. American
805 Mineralogist, 87, 1046–1061.
806 Webster, J.D., Tappen, C.M., and Mandeville, C.W. (2009) Partitioning behavior of
807 chlorine and fluorine in the system apatite–melt–fluid. II: Felsic silicate systems at
808 200MPa. Geochimica et Cosmochimica Acta, 73, 559–581.
809 Workman, R.K., Hauri, E., Hart, S.R., Wang, J., and Blusztajn, J. (2006) Volatile and
810 trace elements in basaltic glasses from Samoa: Implications for water distribution in

811 the mantle. Earth and Planetary Science Letters, 241, 932–951.
812 Wysoczanski, R.J., Wright, I.C., Gamble, J.A., Hauri, E.H., Luhr, J.F., Eggins, S.M., and
813 Handler, M.R. (2006) Volatile contents of Kermadec Arc–Havre Trough pillow
814 glasses: Fingerprinting slab-derived aqueous fluids in the mantle sources of arc and
815 back-arc lavas. Journal of Volcanology and Geothermal Research, 152, 51–73.
816 Zhu, C., and Sverjensky, D.A. (1991) Partitioning of F-Cl-OH between minerals and
817 hydrothermal fluids. Geochimica et Cosmochimica Acta, 55, 1837–1858.
818 Zhu, C., and Sverjensky, D.A. (1992) F-Cl-OH partitioning between biotite and apatite.
819 Geochimica et Cosmochimica Acta, 56, 3435–3467.
820
821

822 Figure 1 Representative BSE images of quenched experimental charges: (a) exp. C3269
823 and (b) exp. C4058, showing bubble-free glasses quenched from melts at 2.5 GPa, 800°C.
824 Mineral abbreviations: Ap, apatite; Bi, biotite; Grt, garnet; Ky, kyanite; Q, quartz.
825
826 Figure 2 a) Agreement between SEM EDS, EMP WDS analytical results (black symbols)
827 and mass balance estimates (grey symbols) for Cl content in melt. The grouping of data is
828 based on bulk Cl and F contents in the EPSM starting compositions, "Cl",
829 "Cl+700ppmF" and "Cl+1500ppmF". The mass balance estimate for Cl content of melt
830 from exp. C4049 lies above the 1:1 line, suggesting the actual bulk Cl content in exp.
831 C4049 is lower than intended. b) Cl content in melt (SEM EDS analytical results plotted)
832 shows a linear increase with the bulk Cl content in EPSM. The data point for exp. C4049
833 falls off the trend defined by other data points. This trend also suggests an estimated
834 ~3000 ppm bulk Cl for exp. C4049. C) Comparison of EMP EDS analytical results for F
835 content in melt with mass balance estimates. The data point for exp. C4049 lies above the
836 1:1 line, suggesting the actual bulk F content in exp. C4049 is lower than intended.
837
838 Figure 3 Mole fractions of (a) Cl, (b) OH and (c) F in apatite show systematic change
839 with the bulk F and Cl content in EPSM. Their variation with the bulk F content can be
840 seen by comparing the three data groups "Cl", "Cl+700ppmF" and "Cl+1500ppmF".
841 Note the estimated bulk Cl content ~3000 ppm has been used for exp. C4049.
842
843 Figure 4 Cl contents in (a) apatite, (b) phengite (small symbols) and biotite (big symbols)
844 show linear correlations with Cl content in melt. Cl partition coefficients between apatite

845 and melt ($D_{Cl}^{Ap\text{-}melt}$) have been determined by linear regression for the three data groups
846 "Cl", "Cl+700ppmF", and "Cl+1500ppmF", respectively. Uniform Cl partition
847 coefficients between phengite and melt ($D_{Cl}^{Phen\text{-}melt}$) and biotite and melt ($D_{Cl}^{Bi\text{-}melt}$) were
848 derived from linear regression of the entire data set.
849
850 Figure 5 F contents in (a) phengite and biotite show linear correlation with F content in
851 melt, while F content in (b) apatite has a non-linear correlation with F content in melt. F
852 partition coefficients between phengite and melt ($D_{F}^{Phen\text{-}melt}$) and biotite and melt ($D_{F}^{Bi\text{-}melt}$)
853 were determined by linear regression. Note that the data point for phengite of exp. D1218
854 appears as an outlier, and is thus not included in the regression.
855
856 Figure 6 Linear Regressions based on equations (a) (9), (b) (14) and (c) (17) for modeling
857 non-ideal mixing of F, Cl and OH in the apatite ternary solution at 2.5 GPa, 800°C.
858
859 Figure 7 F and Cl budgets based on analytical results for F and Cl contents in melt,
860 apatite, phengite and biotite, and the mass fraction of each phase derived from mass
861 balance calculations.
862
863 Figure 8 Linear regressions based on equations (a) (9), (b) (19), (c) (20), (d) (21), (e)
864 (22.1) and (f) (22.2) for modeling non-ideal mixing of F, Cl and OH in apatite at 0.2 GPa,
865 900°C based on the data of Webster et al. (2009). The regressions for 0.05 GPa, 900°C
866 experiments from Doherty et al. (2014) are based on equations (g) (20) and (h) (21).
867

868 Figure 9 (a) Linear correlation between melt Cl content and the molar ratio $X_{\mathrm{Cl}}^{\mathrm{melt}} / X_{\mathrm{OH}}^{\mathrm{melt}}$
869 for EPSM-1, 2 and 5 experiments from Li and Hermann (2015) covering the *PT* range
870 2.5-4.5 GPa and 690-900°C. Similar linear correlations between Cl content in melt and
871 the molar ratio $X_{\mathrm{Cl}}^{\mathrm{melt}} / X_{\mathrm{OH}}^{\mathrm{melt}}$ are also observed for (b) 1 GPa, ~1000°C experiments from
872 McCubbin et al. (2015) and (c) 0.2 GPa, ~900°C experiments from Webster et al. (2009).
873 (d) Linear correlation between F content in melt and the molar ratio $X_{\mathrm{F}}^{\mathrm{melt}} / X_{\mathrm{OH}}^{\mathrm{melt}}$ for 0.2
874 GPa, ~900°C experiments from Webster et al. (2009).
875
876 Figure 10 Excellent agreement between calculated Cl content in melt using equations
877 (26.1) and (27) and estimated values from Webster et al. (2009) based on Cl partitioning
878 data.
879

Table 1 The anhydrous composition of experimental pelite starting material (EPSM) with comparison to the average composition of "Global Subducting Sediment" (GLOSS, Plank and Langmuir 1998) in both hydrous and anhydrous forms, and the average composition of upper continental crust (UCC, Taylor and McLennan 1985; Rudnick and Gao 2003).

wt%	EPSM	GLOSS (P&L98)	GLOSS (P&L98)	UCC (T&M85)	UCC (R&G03)
SiO_2	68.49	58.57	65.28	65.89	66.62
TiO_2	0.67	0.62	0.69	0.50	0.64
Al_2O_3	14.63	11.91	13.27	15.17	15.40
FeO	4.65	5.21	5.81	4.49	5.04
MnO	0.11	0.32	0.36	0.07	0.10
MgO	2.50	2.48	2.76	2.20	2.48
CaO	2.44	5.95	6.63	4.19	3.59
Na_2O	2.61	2.43	2.71	3.89	3.27
K_2O	2.93	2.04	2.27	3.39	2.80
P_2O_5	1.00	0.19	0.21	0.20	0.15
H_2O		7.29			
F (ppm)					557
Total	100.00	97.01	100.00	99.99	100.09

Table 2 Bulk H_2O, Cl and F contents for each experimental run and resultant phase assemblages.

Run no.	Starting Comp.	H_2O (wt%)	Cl (wt%)	F (wt%)	Ap	melt	Ky	Q	Grt	Phen	Bi
C3269	EPSM-1	6.64	0.08		1.2	57	1.5	17	19	5	
C3922	EPSM-2	6.68	0.21		1.5	57	0.5	15	18	9	
C3927	EPSM-3	6.74		0.07	1.8	52	0.4	18	17	11	
C3955	EPSM-4	6.46	0.065	0.09	1.9	48	1	20	16	11	3
D1218	EPSM-5	6.29	0.19	0.07	1.6	55	2	17	17	8	
D1222	EPSM-6	7.02	0.07		1.4	53	0	18	17	11	
C4049	EPSM-8	7.16	0.41[a]	0.07	1.4	62	1.5	14	16	5	
C4059	EPSM-9	7.16	0.22	0.15	1.6	57	1	16	15	7	3
C4058	EPSM-10	7.17	0.11	0.15	1.7	54	0	17	16	10	2

Note: The numbers in the columns with mineral abbreviations or "melt" as headers are estimated mass fractions (in %) for mineral and melt phases, based on mass balance of major elements. Mineral abbreviations: Ap, apatite; Bi, biotite; Grt, garnet; Ky, kyanite; Phen, phengite; Q, quartz.

[a]This is the intended Cl content for EPSM-8. The actual Cl content is estimated to be ~0.3 wt%, see text for details.

Table 3 Melt compositions: analytical, mass balance and modeling results.

Run no.	[a]C3269		[a]C3922		D1222		C3927		C3955	
Starting Comp.	EPSM-1		EPSM-2		EPSM-6		EPSM-3		EPSM-4	
		[b]σ(8)		σ(5)		σ(5)		σ(5)		σ(6)
SiO_2	63.60	*0.64*	64.47	*0.58*	62.64	*0.28*	64.91	*1.03*	63.42	*0.36*
TiO_2	0.22	*0.04*	0.17	*0.07*	0.21	*0.12*	0.15	*0.03*	0.22	*0.05*
Al_2O_3	12.42	*0.32*	12.58	*0.18*	12.73	*0.08*	12.63	*0.10*	12.59	*0.11*
FeO	0.54	*0.07*	0.57	*0.11*	0.48	*0.07*	0.33	*0.09*	0.42	*0.10*
MgO	0.39	*0.04*	0.38	*0.03*	0.42	*0.03*	0.39	*0.02*	0.35	*0.10*
CaO	0.87	*0.05*	0.72	*0.07*	0.68	*0.03*	0.64	*0.04*	0.62	*0.04*
Na_2O	3.12	*0.51*	3.75	*0.42*	4.12	*0.14*	4.30	*0.10*	4.64	*0.15*
K_2O	3.33	*0.10*	3.09	*0.10*	3.07	*0.04*	3.04	*0.05*	2.76	*0.06*
P_2O_5	0.29	*0.04*	0.32	*0.07*	0.35	*0.04*	0.20	*0.04*	0.19	*0.06*
Cl	0.08	*0.02*	0.26	*0.01*	0.07	*0.02*			0.11	*0.02*
Total	84.85	*0.93*	86.30	*0.46*	84.90	*0.56*	86.60	*1.08*	85.30	*0.68*
		σ(9)		σ(4)		σ(5)		σ(4)		σ(6)
[c]Cl(EMPA)	0.09	*0.01*	0.33	*0.02*	0.07	*0.01*			0.10	*0.01*
[c]F(EMPA)							0.04	*0.01*	0.06	*0.01*
[d]Si/Al	4.35		4.36		4.18		4.37		4.28	
[d]Na+K/Al	0.70		0.76		0.79		0.82		0.84	
Mass balance results										
Cl wt%	0.12	*0.02*	0.28	*0.05*	0.11	*0.02*			0.11	*0.02*
H_2O wt%	11	*2*	11	*2*	12	*2*	12	*2*	12	*3*
F wt%							0.05	*0.01*	0.07	*0.01*
[e]Modeling after Silver and Stolper (1985) and Hui et al. (2008)										
W	32.43		32.51		32.54		*32.43*		32.52	
K_1	0.34		0.34		0.34		0.34		0.34	
X_{H2Ot}	0.19	*0.03*	0.18	*0.03*	0.20	*0.04*	0.20	*0.04*	0.20	*0.04*
X_{H2Om}	0.11	*0.04*	0.10	*0.04*	0.11	*0.04*	0.11	*0.04*	0.11	*0.05*
X_O	0.73	*0.04*	0.74	*0.04*	0.72	*0.04*	0.72	*0.04*	0.72	*0.05*
X_{OH}	0.16	*0.03*	0.16	*0.03*	0.17	*0.03*	0.17	*0.03*	0.17	*0.03*
X_{Cl}	0.0007	*0.0002*	0.0022	*0.0001*	0.0006	*0.0002*			0.0009	*0.0002*
X_F							0.0006	*0.0001*	0.0009	*0.0001*

Table 3 (continued)

Run no.	[a]D1218		C4049		C4058		C4059	
Starting Comp.	EPSM-5		EPSM-8		EPSM-10		EPSM-9	
		[b]*σ(4)*		*σ(5)*		*σ(6)*		*σ(6)*
SiO_2	63.78	*0.03*	63.48	*0.27*	63.13	*0.36*	62.38	*0.20*
TiO_2	0.20	*0.06*	0.19	*0.03*	0.23	*0.04*	0.19	*0.03*
Al_2O_3	12.16	*0.11*	12.30	*0.12*	12.55	*0.07*	12.22	*0.06*
FeO	0.65	*0.10*	0.73	*0.05*	0.56	*0.05*	0.65	*0.06*
MgO	0.49	*0.03*	0.60	*0.02*	0.49	*0.06*	0.63	*0.04*
CaO	0.95	*0.06*	1.11	*0.04*	0.82	*0.03*	0.95	*0.04*
Na_2O	3.04	*0.11*	3.41	*0.06*	4.23	*0.10*	4.00	*0.15*
K_2O	3.56	*0.04*	3.48	*0.05*	2.78	*0.04*	2.88	*0.03*
P_2O_5	0.31	*0.05*	0.38	*0.05*	0.26	*0.06*	0.30	*0.05*
Cl	0.23	*0.02*	0.39	*0.04*	0.15	*0.03*	0.28	*0.02*
Total	85.36	*0.13*	86.06	*0.27*	85.19	*0.57*	84.48	*0.32*
		σ(3)		*σ(3)*		*σ(5)*		*σ(5)*
[c]Cl(EMPA)	0.22	*0.01*	0.36	*0.06*	0.16	*0.01*	0.30	*0.05*
[c]F(EMPA)	0.03	*0.004*	0.02	*0.01*	0.15	*0.01*	0.15	*0.01*
[d]Si/Al	4.46		4.39		4.27		4.34	
[d]Na+K/Al	0.73		0.76		0.79		0.79	
Mass balance results								
Cl wt%	0.32	*0.06*	0.62	*0.10*	0.18	*0.03*	0.35	*0.06*
H_2O wt%	11	*2*	11	*2*	12	*2*	12	*2*
F wt%	0.06	*0.01*	0.07	*0.01*	0.14	*0.03*	0.14	*0.02*
[e]Modeling after Silver and Stolper (1985) and Hui et al. (2008)								
W	*32.56*		32.72		32.54		32.64	
K_1	0.34		0.34		0.34		0.34	
X_{H2Ot}	0.18	*0.03*	0.18	*0.03*	0.20	*0.04*	0.20	*0.04*
X_{H2Om}	0.10	*0.04*	0.10	*0.03*	0.11	*0.04*	0.11	*0.04*
X_O	0.74	*0.04*	0.74	*0.03*	0.72	*0.04*	0.72	*0.04*
X_{OH}	0.16	*0.03*	0.16	*0.02*	0.17	*0.03*	0.17	*0.03*
X_{Cl}	0.0019	*0.0002*	0.0033	*0.0004*	0.0013	*0.0003*	0.0024	*0.0002*
X_F	0.0005	*0.0001*	0.0003	*0.0001*	0.0024	*0.0002*	0.0024	*0.0001*

[a]This experiment was previously reported in Li and Hermann (2015), and is relisted here for ease of comparison.

[b]The standard deviation of multiple analyses; number of analyses shown in brackets.

[c]Cl and F contents in melt obtained from EMP WDS analysis.

[d]These are molar ratios.

[e]Hydrous silicate melts are modeled as ideal mixtures of water molecules (H_2O_m), OH, O, Cl and F following the work of Silver and Stolper (1985). *W* (in g/mol) is the molar weight of anhydrous silicate per oxygen for melt. K_1 is the equilibrium constant for the reaction H_2O_m (melt) + O (melt) = 2OH (melt), calculated based on Hui et al. (2008); X_{H2Ot}, X_{OH}, X_{H2Om}, X_O, X_{Cl} and X_F are the mole fractions of total H_2O, OH, H_2O_m, O, Cl and F, respectively. For further details see appendix C of Li and Hermann (2015).

914 Table 4 Apatite compositions and resultant partition and exchange coefficients.
915

Run no.	[a]C3269		[a]C3922		D1222		C3927		C3955	
Starting Comp.	EPSM-1		EPSM-2		EPSM-6		EPSM-3		EPSM-4	
		[b]σ(10)		σ(6)		σ(6)		σ(5)		σ(7)
SiO_2	1.11	*0.24*	0.69	*0.23*	0.67	*0.29*	0.66	*0.09*	0.74	*0.24*
Al_2O_3	0.24	*0.15*	0.13	*0.05*	0.17	*0.09*	0.12	*0.04*	0.17	*0.05*
FeO	0.86	*0.14*	1.04	*0.09*	0.97	*0.12*	0.59	*0.08*	0.74	*0.10*
MgO	0.58	*0.06*	0.65	*0.03*	0.68	*0.04*	0.50	*0.07*	0.43	*0.08*
CaO	49.86	*0.79*	49.59	*0.36*	50.34	*0.16*	50.40	*1.22*	50.79	*0.49*
Na_2O	0.35	*0.08*	0.41	*0.11*	0.42	*0.11*	0.42	*0.26*	0.65	*0.17*
K_2O	0.18	*0.07*	0.15	*0.04*	0.11	*0.05*	0.15	*0.05*	0.15	*0.05*
P_2O_5	41.61	*0.63*	39.72	*0.14*	40.91	*0.33*	39.53	*0.91*	40.37	*0.47*
Cl	1.20	*0.07*	2.67	*0.06*	0.91	*0.03*			0.33	*0.02*
								σ(20)		*σ(15)*
[c]F(EMPA)							2.02	*0.14*	2.05	*0.08*
Less O=F							-0.85		-0.86	
Less O=Cl	-0.27		-0.60		-0.20				-0.07	
Total	95.71	*1.41*	94.44	*0.51*	94.97	*0.21*	93.55	*2.27*	95.48	*0.93*
Apatite structure formula based on 12.5 O^{2-}										
Si	0.095	*0.020*	0.061	*0.020*	0.058	*0.025*	0.059	*0.008*	0.064	*0.021*
Al	0.024	*0.015*	0.013	*0.005*	0.017	*0.010*	0.013	*0.005*	0.018	*0.005*
Fe	0.062	*0.010*	0.077	*0.007*	0.070	*0.009*	0.044	*0.006*	0.054	*0.007*
Mg	0.073	*0.008*	0.086	*0.004*	0.088	*0.005*	0.066	*0.008*	0.056	*0.010*
Ca	4.568	*0.030*	4.706	*0.034*	4.667	*0.021*	4.789	*0.031*	4.736	*0.037*
Na	0.058	*0.014*	0.070	*0.019*	0.071	*0.018*	0.072	*0.044*	0.109	*0.029*
K	0.019	*0.008*	0.017	*0.005*	0.013	*0.006*	0.017	*0.006*	0.017	*0.005*
P	3.013	*0.017*	2.978	*0.013*	2.997	*0.024*	2.968	*0.005*	2.974	*0.012*
Tot.Cat.	7.912	*0.017*	8.007	*0.011*	7.980	*0.019*	8.027	*0.024*	8.028	*0.022*
F							0.567	*0.040*	0.565	*0.024*
Cl	0.173	*0.009*	0.401	*0.009*	0.133	*0.005*			0.048	*0.004*
OH	0.827	*0.009*	0.599	*0.009*	0.867	*0.005*	0.433	*0.040*	0.387	*0.024*
[d]X_F							0.537	*0.036*	0.545	*0.022*
[d]X_{Cl}	0.176	*0.011*	0.392	*0.008*	0.133	*0.005*			0.048	*0.004*
[d]X_{OH}	0.824	*0.011*	0.608	*0.008*	0.867	*0.005*	0.463	*0.036*	0.407	*0.023*
Partition and exchange coefficients										
[e]C_{Cl}^{melt} wt%	0.09	0.01	0.26	*0.01*	0.07	*0.01*			0.11	*0.02*
$D_{Cl}^{Ap\text{-}melt}$	13.8	*1.3*	10.1	*0.6*	12.4	*2.2*			3.1	*0.7*
$K_{d\,Cl\text{-}OH}^{Ap\text{-}melt}$	47	*9*	49	*9*	42	*11*			23	*7*
[f]C_F^{melt} wt%							0.04	*0.01*	0.06	*0.01*
$D_F^{Ap\text{-}melt}$							51	*11*	34	*4*
$K_{d\,F\text{-}OH}^{Ap\text{-}melt}$							353	*105*	256	*62*
$K_{d\,F\text{-}Cl}^{Ap\text{-}melt}$									11	*3*

916

Table 4 (continued)

Run no.	[a]D1218		C4049		C4058		C4059	
Starting Comp.	EPSM-5		EPSM-8		EPSM-10		EPSM-9	
		σ(8)		*σ(6)*		*σ(6)*		*σ(6)*
SiO_2	0.62	*0.19*	0.55	*0.08*	0.72	*0.20*	0.82	*0.41*
Al_2O_3	0.13	*0.03*	0.10	*0.04*	0.13	*0.04*	0.16	*0.06*
FeO	0.91	*0.11*	1.11	*0.14*	0.71	*0.14*	0.86	*0.08*
MgO	0.67	*0.08*	0.62	*0.07*	0.45	*0.06*	0.47	*0.07*
CaO	51.61	*0.37*	50.98	*0.43*	51.06	*0.48*	50.75	*0.50*
Na_2O	0.25	*0.10*	0.24	*0.04*	0.31	*0.16*	0.27	*0.05*
K_2O	0.12	*0.04*	0.15	*0.03*	0.17	*0.06*	0.16	*0.05*
P_2O_5	40.68	*0.24*	42.52	*0.45*	42.13	*0.40*	41.87	*0.48*
Cl	0.88	*0.02*	1.33	*0.04*	0.34	*0.02*	0.51	*0.01*
		σ(21)		*σ(24)*		*σ(20)*		*σ(20)*
[c]F(EMPA)	1.71	*0.10*	1.57	*0.16*	2.49	*0.16*	2.38	*0.15*
Less O=F	-0.72		-0.66		-1.05		-1.00	
Less O=Cl	-0.20		-0.30		-0.08		-0.12	
Total	96.66	*0.62*	98.20	*0.97*	97.38	*1.12*	97.12	*0.52*
Apatite structure formula based on 12.5 O^{2-}								
Si	0.053	*0.016*	0.046	*0.007*	0.061	*0.017*	0.070	*0.035*
Al	0.013	*0.003*	0.008	*0.005*	0.013	*0.004*	0.016	*0.006*
Fe	0.066	*0.008*	0.079	*0.010*	0.050	*0.010*	0.061	*0.006*
Mg	0.086	*0.010*	0.078	*0.008*	0.057	*0.008*	0.060	*0.009*
Ca	4.768	*0.026*	4.613	*0.024*	4.645	*0.017*	4.634	*0.033*
Na	0.041	*0.016*	0.039	*0.007*	0.051	*0.025*	0.044	*0.009*
K	0.013	*0.004*	0.016	*0.003*	0.018	*0.007*	0.017	*0.005*
P	2.970	*0.011*	3.040	*0.004*	3.029	*0.013*	3.021	*0.023*
Tot.Cat.	8.012	*0.010*	7.918	*0.011*	7.924	*0.023*	7.922	*0.011*
F	0.465	*0.029*	0.420	*0.044*	0.669	*0.044*	0.641	*0.041*
Cl	0.128	*0.003*	0.190	*0.006*	0.049	*0.003*	0.074	*0.002*
OH	0.407	*0.029*	0.390	*0.044*	0.282	*0.044*	0.285	*0.041*
[d]X_F	0.453	*0.028*	0.417	*0.043*	0.661	*0.043*	0.631	*0.039*
[d]X_{Cl}	0.129	*0.003*	0.195	*0.005*	0.050	*0.003*	0.075	*0.002*
[d]X_{OH}	0.419	*0.028*	0.387	*0.044*	0.289	*0.043*	0.294	*0.039*
Partition and exchange coefficients								
[e]C_{Cl}^{melt} wt%	0.22	*0.02*	0.39	*0.04*	0.15	*0.03*	0.28	*0.02*
$D_{Cl}^{Ap\text{-}melt}$	3.9	*0.4*	3.4	*0.4*	2.3	*0.5*	1.8	*0.2*
$K_{d\,Cl\text{-}OH}^{Ap\text{-}melt}$	27	*6*	25	*5*	24	*8*	19	*5*
[f]C_F^{melt} wt%	0.03	*0.004*	0.02	*0.01*	0.15	*0.01*	0.15	*0.01*
$D_F^{Ap\text{-}melt}$	51	*7*	72	*22*	16	*1*	16	*1*
$K_{d\,F\text{-}OH}^{Ap\text{-}melt}$	343	*78*	512	*184*	173	*44*	164	*39*
$K_{d\,F\text{-}Cl}^{Ap\text{-}melt}$	13	*2*	21	*7*	7	*2*	9	*1*

[a]This experiment was previously reported in Li and Hermann (2015), and is relisted here for ease of comparison.
[b]The standard deviation of multiple analyses; number of analyses shown in brackets.
[c]F and Cl contents obtained from EMP WDS analysis.
[d]Mole fractions of F and Cl in apatite are calculated using the method of Piccoli and Candela (2002) with the equations: $X_F^{Ap}=C_F^{Ap}/3.767$ and $X_{Cl}^{Ap}=C_{Cl}^{Ap}/6.809$, where X_F^{Ap} & X_{Cl}^{Ap} are the mole fractions of FAp and ClAp, and C_F^{Ap} & C_{Cl}^{Ap} are the concentrations of F and Cl in apatite in wt%.
[e]Cl content in melt obtained from SEM EDS analysis if >0.1 wt%, and EMP WDS analysis if <0.1 wt%.
[f]F content in melt obtained from EMP WDS analysis.

929 Table 5 Phengite compositions and resultant partition and exchange coefficients.
930

Run no.	[a]C3269		[a]C3922		D1222		C3927		C3955	
Starting Comp.	EPSM-1		EPSM-2		EPSM-6		EPSM-3		EPSM-4	
		[b]σ(5)		σ(6)		σ(4)		σ(5)		σ(5)
SiO_2	47.17	*0.79*	47.81	*1.07*	47.47	*0.53*	44.80	*4.39*	48.12	*0.68*
TiO_2	1.88	*0.17*	1.62	*0.18*	1.55	*0.13*	1.58	*0.23*	1.56	*0.09*
Al_2O_3	26.87	*0.99*	28.02	*1.18*	26.69	*0.65*	25.94	*2.35*	27.11	*0.50*
FeO	1.33	*0.26*	1.47	*0.18*	1.91	*0.25*	1.62	*0.21*	1.55	*0.12*
MgO	4.75	*0.42*	4.39	*0.37*	4.50	*0.35*	4.65	*0.42*	4.57	*0.14*
Na_2O	0.67	*0.11*	1.03	*0.22*	1.67	*0.45*	1.01	*0.17*	1.42	*0.20*
K_2O	9.65	*0.38*	9.89	*0.40*	9.25	*0.31*	9.23	*0.81*	9.54	*0.16*
Cl									0.032	*0.013*
Total	92.32	*1.71*	94.23	*0.29*	93.03	*1.08*	88.83	*8.26*	93.90	*0.66*
		σ(3)		σ(6)		σ(5)				σ(5)
[c]Cl(EMPA)	0.022	*0.002*	0.058	*0.010*	0.016	*0.005*			0.025	*0.006*
								σ(8)		σ(8)
[c]F(EMPA)							0.08	*0.03*	0.09	*0.02*
Structure formula based on $11O^{2-}$										
Si	3.250	*0.023*	3.233	*0.070*	3.259	*0.033*	3.220	*0.033*	3.266	*0.029*
Ti	0.097	*0.007*	0.082	*0.009*	0.080	*0.007*	0.085	*0.006*	0.080	*0.005*
Al	2.181	*0.044*	2.233	*0.091*	2.159	*0.043*	2.199	*0.037*	2.169	*0.039*
Fe	0.077	*0.016*	0.083	*0.010*	0.109	*0.014*	0.098	*0.011*	0.088	*0.007*
Mg	0.488	*0.051*	0.442	*0.038*	0.460	*0.036*	0.500	*0.028*	0.462	*0.017*
Na	0.090	*0.016*	0.135	*0.029*	0.222	*0.059*	0.141	*0.015*	0.187	*0.025*
K	0.848	*0.021*	0.853	*0.036*	0.810	*0.027*	0.847	*0.021*	0.826	*0.017*
Tot. Cat.	7.031	*0.017*	7.062	*0.031*	7.098	*0.026*	7.089	*0.025*	7.077	*0.013*
Cl	0.003	*0.000*	0.007	*0.001*	0.002	*0.001*			0.003	*0.001*
F							0.018	*0.007*	0.019	*0.005*
OH	1.997	*0.000*	1.993	*0.001*	1.998	*0.001*	1.982	*0.007*	1.979	*0.005*
Partition and exchange coefficients										
[e]C_{Cl}^{melt} wt%	0.09	0.01	0.26	*0.01*	0.07	*0.01*			0.11	*0.02*
$D_{Cl}^{Phen\text{-}melt}$	0.25	*0.03*	0.22	*0.04*	0.22	*0.08*			0.24	*0.08*
[f]C_F^{melt} wt%							0.04	*0.01*	0.06	*0.01*
$D_F^{Phen\text{-}melt}$							2.0	*0.9*	1.4	*0.4*
$K_{d\,Cl\text{-}OH}^{Phen\text{-}melt}$	0.28	*0.06*	0.24	*0.06*	0.26	*0.12*			0.27	*0.10*
$K_{d\,F\text{-}OH}^{Phen\text{-}melt}$									6	*3*
$K_{d\,F\text{-}Cl}^{Phen\text{-}melt}$							2	*1*	1.7	*0.6*

931
932
933

Table 5 (continued)

Run no.	[a]D1218		C4049		C4058		C4059	
Starting Comp.	EPSM-5		EPSM-8		EPSM-10		EPSM-9	
		σ(6)		*σ(4)*		*σ(5)*		*σ(4)*
SiO_2	47.58	*0.71*	47.04	*0.62*	47.97	*1.12*	47.18	*0.24*
TiO_2	1.54	*0.21*	1.47	*0.15*	1.44	*0.12*	1.16	*0.13*
Al_2O_3	26.84	*0.61*	27.37	*0.49*	27.32	*0.91*	27.78	*0.40*
FeO	1.41	*0.27*	2.32	*0.32*	1.92	*0.55*	2.23	*0.34*
MgO	5.11	*0.76*	5.21	*0.37*	4.42	*0.19*	4.06	*0.42*
Na_2O	0.46	*0.02*	0.47	*0.05*	1.09	*0.42*	0.68	*0.09*
K_2O	9.82	*0.23*	9.97	*0.14*	9.54	*0.37*	9.85	*0.23*
Cl	0.042	*0.023*	0.123	*0.022*	0.056	*0.025*	0.085	*0.013*
Total	92.80	*0.39*	93.95	*0.67*	93.76	*0.94*	93.03	*0.25*
		σ(5)		*σ(6)*		*σ(5)*		*σ(7)*
[c]Cl(EMPA)	0.054	*0.006*	0.101	*0.012*	0.043	*0.006*	0.061	*0.014*
[c]F(EMPA)	0.15	*0.02*	0.04	*0.02*	0.19	*0.02*	0.22	*0.04*
Structure formula based on $11O^{2-}$								
Si	3.263	*0.027*	3.210	*0.019*	3.262	*0.073*	3.242	*0.010*
Ti	0.079	*0.011*	0.075	*0.008*	0.074	*0.006*	0.060	*0.007*
Al	2.168	*0.036*	2.201	*0.028*	2.190	*0.069*	2.250	*0.030*
Fe	0.081	*0.016*	0.132	*0.019*	0.109	*0.031*	0.128	*0.020*
Mg	0.523	*0.080*	0.530	*0.040*	0.448	*0.020*	0.416	*0.043*
Na	0.061	*0.003*	0.062	*0.006*	0.143	*0.055*	0.091	*0.012*
K	0.859	*0.023*	0.868	*0.012*	0.828	*0.031*	0.864	*0.019*
Tot. Cat.	7.034	*0.055*	7.079	*0.030*	7.055	*0.028*	7.050	*0.005*
Cl	0.006	*0.001*	0.012	*0.001*	0.005	*0.001*	0.007	*0.002*
F	0.032	*0.003*	0.009	*0.004*	0.041	*0.005*	0.047	*0.008*
OH	1.962	*0.003*	1.979	*0.004*	1.954	*0.005*	1.946	*0.008*
Partition and exchange coefficients								
[e]C_{Cl}^{melt} wt%	0.22	*0.02*	0.39	*0.04*	0.15	*0.03*	0.28	*0.02*
$D_{Cl}^{Phen\text{-}melt}$	0.24	*0.04*	0.26	*0.04*	0.29	*0.07*	0.22	*0.05*
[f]C_F^{melt} wt%	0.03	*0.004*	0.02	*0.01*	0.15	*0.01*	0.15	*0.01*
$D_F^{Phen\text{-}melt}$	4.4	*0.7*	1.9	*1.0*	1.2	*0.2*	1.4	*0.2*
$K_{d\,Cl\text{-}OH}^{Phen\text{-}melt}$	0.27	*0.06*	0.29	*0.06*	0.34	*0.10*	0.26	*0.08*
$K_{d\,F\text{-}OH}^{Phen\text{-}melt}$	18	*4*	7	*4*	4	*1*	7	*2*
$K_{d\,F\text{-}Cl}^{Phen\text{-}melt}$	5	*1*	2	*1*	1.5	*0.3*	1.7	*0.4*

Footnotes are the same as those for Table 4.

939 Table 6 Biotite compositions and resultant partition and exchange coefficients.
940

Run no.	C3955		C4059		C4058	
Starting Comp.	EPSM-4		EPSM-9		EPSM-10	
		[b]σ(3)		σ(2)		σ(2)
SiO_2	41.96	*0.78*	41.27	*0.01*	42.33	*0.40*
TiO_2	2.64	*0.13*	2.70	*0.20*	2.76	*0.40*
Al_2O_3	17.60	*0.21*	17.44	*0.83*	18.26	*0.36*
FeO	5.40	*0.27*	5.53	*0.09*	5.32	*0.15*
MgO	15.58	*0.45*	15.80	*0.33*	15.09	*0.21*
Na_2O	0.94	*0.27*	0.85	*0.13*	1.32	*0.47*
K_2O	9.19	*0.17*	9.20	*0.40*	9.14	*0.21*
Cl	0.087	*0.015*	0.235	*0.007*	0.135	*0.007*
Total	93.77	*0.91*	93.01	*1.08*	94.33	*0.45*
		σ(6)		σ(4)		σ(3)
[c]Cl(EMPA)	0.102	*0.011*	0.228	*0.018*	0.146	*0.005*
		σ(5)				
[c]F(EMPA)	0.30	*0.02*	0.48	*0.04*	0.60	*0.03*
Structure formula based on $11O^{2-}$						
Si	3.007	*0.024*	2.981	*0.028*	3.002	*0.039*
Ti	0.142	*0.007*	0.147	*0.009*	0.147	*0.021*
Al	1.486	*0.020*	1.484	*0.056*	1.526	*0.025*
Fe	0.323	*0.018*	0.334	*0.002*	0.315	*0.008*
Mg	1.664	*0.055*	1.702	*0.052*	1.595	*0.017*
Na	0.131	*0.036*	0.118	*0.020*	0.182	*0.065*
K	0.840	*0.017*	0.847	*0.029*	0.826	*0.016*
Tot. Cat.	7.594	*0.009*	7.613	*0.004*	7.593	*0.019*
Cl	0.012	*0.001*	0.028	*0.002*	0.017	*0.001*
F	0.068	*0.004*	0.109	*0.008*	0.135	*0.007*
OH	1.920	*0.004*	1.863	*0.008*	1.848	*0.007*
Partition and exchange coefficients						
[e]C_{Cl}^{melt} wt%	0.11	*0.02*	0.28	*0.02*	0.15	*0.03*
$D_{Cl}^{Bi\text{-}melt}$	0.97	*0.24*	0.81	*0.09*	0.97	*0.20*
[f]C_F^{melt} wt%	0.06	*0.01*	0.15	*0.01*	0.15	*0.01*
$D_F^{Bi\text{-}melt}$	5.0	*0.7*	3.1	*0.3*	4.0	*0.3*
$K_{d_{Cl\text{-}OH}}^{Bi\text{-}melt}$	1.23	*0.39*	1.06	*0.22*	1.26	*0.34*
$K_{d_{F\text{-}OH}}^{Bi\text{-}melt}$	5	*1*	3.9	*0.6*	4.1	*0.9*
$K_{d_{F\text{-}Cl}}^{Bi\text{-}melt}$	6	*2*	4.1	*0.8*	5	*1*

941 Footnotes are the same as those for Table 4.
942

Table 7 Summary of regression results: Margules parameters for the apatite regular solution model, and the Gibbs free energies of F, Cl and OH exchange reactions between apatite and melt.

P(GPa)	T(°C)	Data source	Data of Regression	$W_{Cl\text{-}OH}$	SE	$W_{F\text{-}OH}$-$W_{F\text{-}Cl}$	SE	$W_{F\text{-}Cl}$	SE	$W_{F\text{-}OH}$	SE	$\Delta_r G^{o\ Ap\text{-}melt}_{Cl\text{-}OH}$	SE	$\Delta_r G^{o\ Ap\text{-}melt}_{F\text{-}Cl}$	SE	$\Delta_r G^{o\ Ap\text{-}melt}_{F\text{-}OH}$	SE
2.5	800	This study	$K_{d\,Cl\text{-}OH}^{Ap\text{-}melt}$, $K_{d\,F\text{-}Cl}^{Ap\text{-}melt}$	0		-10.48	1.11	-13.06	3.40	-23.54	3.57	-34.03	0.49	-19.40	0.76		
2.5	800	This study	$K_{d\,Cl\text{-}OH}^{Ap\text{-}melt}$, $K_{d\,F\text{-}OH}^{Ap\text{-}melt}$	0		-10.48	1.11	-10.84	3.38	-21.32	3.20	-34.03	0.49			-51.14	0.98
0.2	900-924	Webster et al. (2009)	$K_{d\,Cl\text{-}OH}^{Ap\text{-}melt}$, $K_{d\,F\text{-}Cl}^{Ap\text{-}melt}$	0		0		15.15	2.82			-26.54	0.89	-17.19	1.27		
0.2	900-924	Webster et al. (2009)	$K_{d\,Cl\text{-}OH}^{Ap\text{-}melt}$, $K_{d\,F\text{-}OH}^{Ap\text{-}melt}$	0		0				14.84	2.68	-26.54	0.89			-44.76	1.09
0.2	900-924	Webster et al. (2009)	$K_{d\,Cl\text{-}OH}^{Ap\text{-}melt}$, $K_{d\,F\text{-}Cl}^{Ap\text{-}melt}$	17.33	6.22	0		17.72	2.28	17.72	2.28	-25.81	1.05	-13.24	1.03		
0.2	900-924	Webster et al. (2009)	$K_{d\,Cl\text{-}OH}^{Ap\text{-}melt}$, $K_{d\,F\text{-}OH}^{Ap\text{-}melt}$	17.33	6.22	0		21.29	2.96	21.29	2.96	-25.81	1.05			-40.33	1.21
0.05	840-950	Doherty et al. (2014)	$K_{d\,Cl\text{-}OH}^{Ap\text{-}melt}$, $K_{d\,F\text{-}Cl}^{Ap\text{-}melt}$	0		0		19.41	6.72					-16.21	3.35		
0.05	840-950	Doherty et al. (2014)	$K_{d\,Cl\text{-}OH}^{Ap\text{-}melt}$, $K_{d\,F\text{-}OH}^{Ap\text{-}melt}$	0		0				25.26	4.20					-52.16	2.15

Note: The unit for all parameters is kJ/mol. “SE” stands for standard error.

Table 8 Calculation of Cl and F content in felsic melt at 0.2 GPa, 900°C based on natural apatite compositions listed in Table 3 of Webster et al. (2009) using parameters derived from regression of experimental data from Webster et al. (2009). Estimations made based on Cl and F partitioning data by Webster et al. (2009) are also listed for comparison.

	1986 Augustine volcano, Alaska	1976 Augustine volcano, Alaska (no. J-1)	1976 Augustine volcano, Alaska (no. PI-9)	1883 Krakatau volcano, Indonesia	1991 Mt. Pinatubo volcano, Philippines	1981 Mt. St. Helens, Washingtone	Mt. Mazama volcano, Oregon climactic erupt	Santorini volcano, Greece	La´scar volcano, Argentina	Bishop Tuff, California
C_{Cl}^{Ap} (wt%)	2.32	1.75	2.1	0.86	1.17	0.72	0.95	1.04	0.67	0.21
C_{F}^{Ap} (wt%)	1.51	1.29	1.39	2.63	1.46	1.88	1.83	2.38	2.51	2.65
X_{Cl}^{Ap}	0.341	0.257	0.308	0.126	0.172	0.106	0.140	0.153	0.098	0.031
X_{F}^{Ap}	0.401	0.342	0.369	0.698	0.388	0.499	0.486	0.632	0.666	0.703
X_{OH}^{Ap}	0.258	0.401	0.323	0.176	0.441	0.395	0.375	0.215	0.235	0.266
Calc. $K_{d_{Cl\text{-}OH}}^{Ap\text{-}melt}$	16.31	10.92	13.74	12.91	8.74	8.43	9.28	12.60	11.05	9.28
σ	1.95	1.54	1.48	1.45	1.77	1.80	1.71	1.45	1.53	1.71
Calc. C_{Cl}^{melt} (wt%)	0.87	0.63	0.75	0.60	0.48	0.34	0.43	0.61	0.41	0.13
σ	0.11	0.09	0.09	0.07	0.10	0.08	0.08	0.08	0.06	0.03
Calc. $K_{d_{F\text{-}OH}}^{Ap\text{-}melt}$	74.16	49.53	60.93	185.47	51.84	75.00	75.15	145.50	153.59	160.21
σ	81.79	48.11	64.17	151.66	39.80	45.41	49.26	110.26	113.15	121.03
Calc. C_{F}^{melt} (wt%)	0.13	0.11	0.12	0.13	0.10	0.10	0.11	0.12	0.11	0.10
σ	0.14	0.10	0.12	0.11	0.08	0.06	0.07	0.09	0.08	0.08
Estimations from Webster et al. (2009)										
C_{Cl}^{melt} (wt%)	[a]0.76	0.9	0.61	0.73	0.41	[a]0.5	0.54	0.58	[a]0.39	0.1
σ	[a]0.08	0.14	0.09	0.11	0.06	[a]0.15	0.08	0.08	[a]0.07	0.02
C_{F}^{melt} (wt%)	0.07	0.065	0.06	0.12	0.07	0.09	0.09	0.11	0.12	0.12
σ	0.02	0.02	0.02	0.01	0.02	0.02	0.02	0.01	0.01	0.01

[a]Where the estimated Cl content in melt is reported as a range, the listed average and standard deviation are formulated to cover such a range.

This is a preprint, the final version is subject to change, of the American Mineralogist (MSA)
Cite as Authors (Year) Title. American Mineralogist, in press.
(DOI will not work until issue is live.) DOI: http://dx.doi.org/10.2138/am-2017-5891

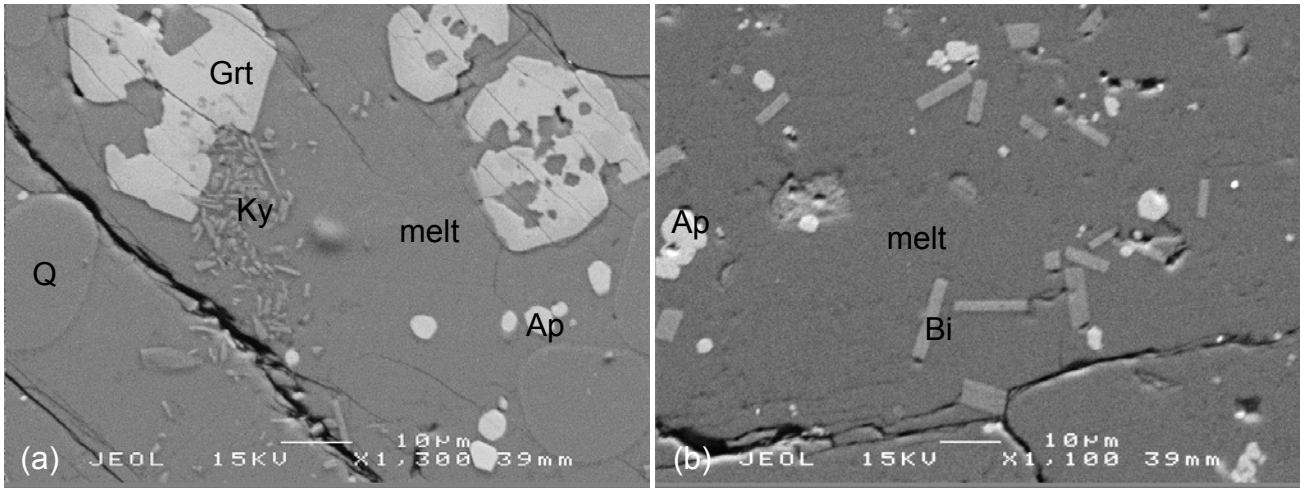

Figure 1

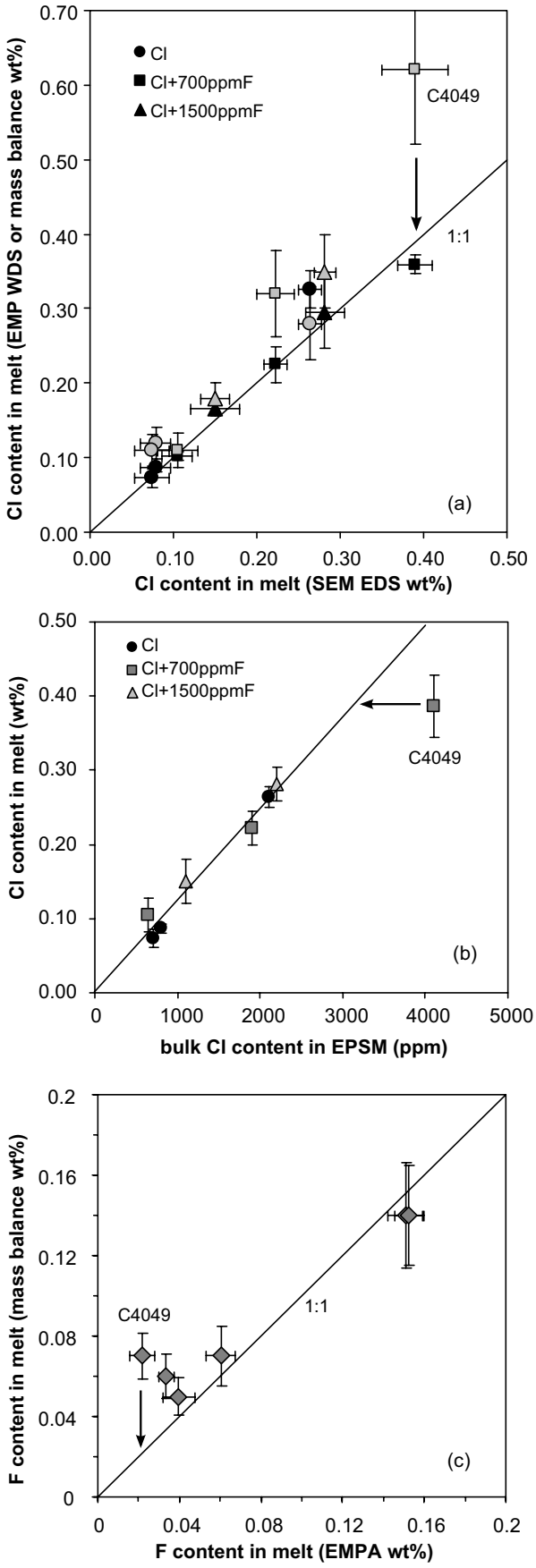
Cl
Cl+700ppmF
Cl+1500ppmF
C4049
1:1
(a)
Cl content in melt (EMP WDS or mass balance wt%)
Cl content in melt (SEM EDS wt%)
0.00
0.10
0.20
0.30
0.40
0.50
0.60
0.70
(b)
Cl content in melt (wt%)
bulk Cl content in EPSM (ppm)
0
1000
2000
3000
4000
5000
(c)
F content in melt (mass balance wt%)
F content in melt (EMPA wt%)
0
0.04
0.08
0.12
0.16
0.2

Figure 2

This is a preprint, the final version is subject to change, of the American Mineralogist (MSA)
Cite as Authors (Year) Title. American Mineralogist, in press.
(DOI will not work until issue is live.) DOI: http://dx.doi.org/10.2138/am-2017-5891

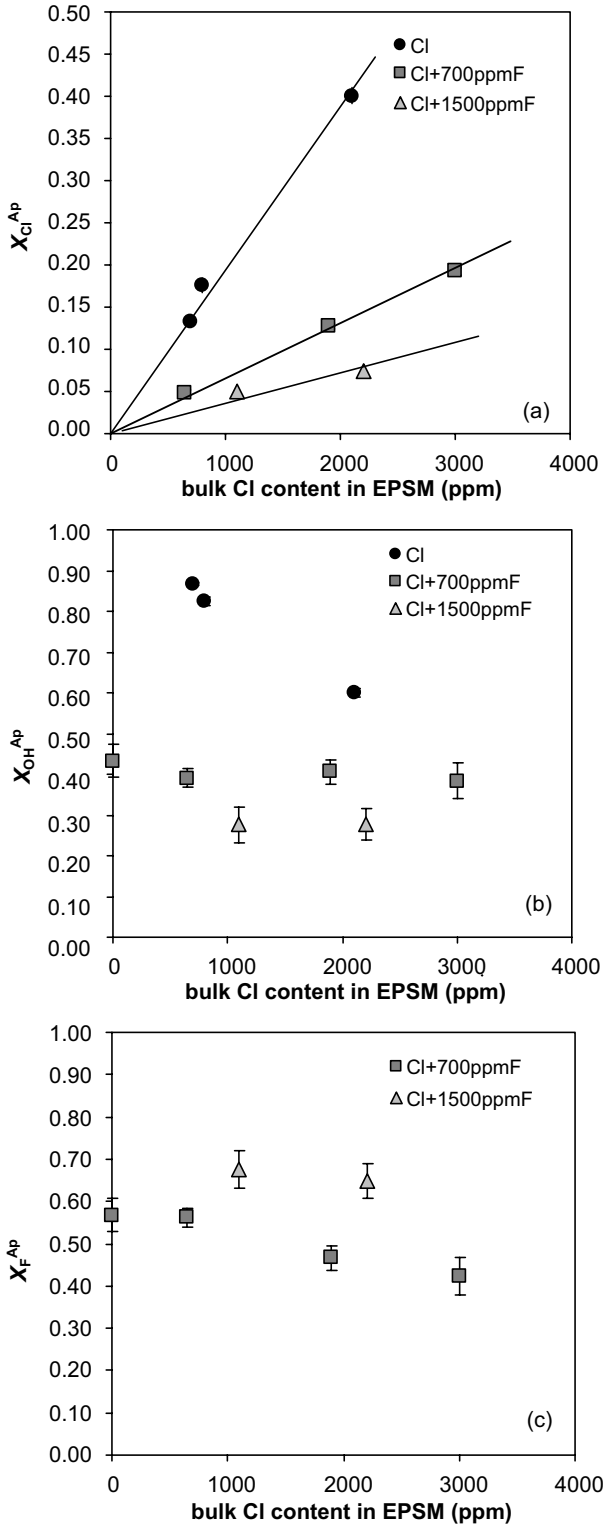

Figure 3

This is a preprint, the final version is subject to change, of the American Mineralogist (MSA)
Cite as Authors (Year) Title. American Mineralogist, in press.
(DOI will not work until issue is live.) DOI: http://dx.doi.org/10.2138/am-2017-5891

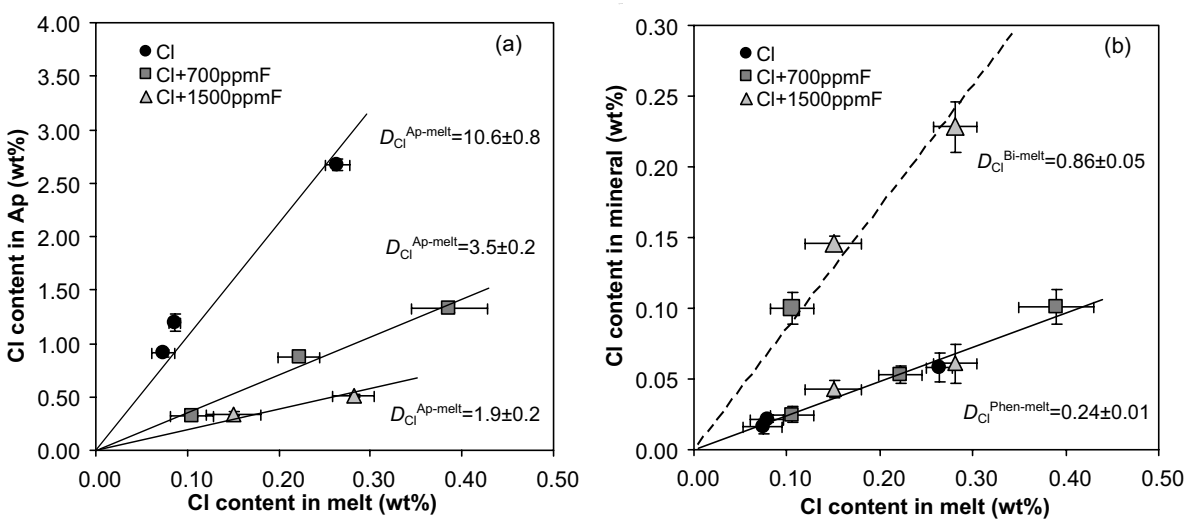

Figure 4

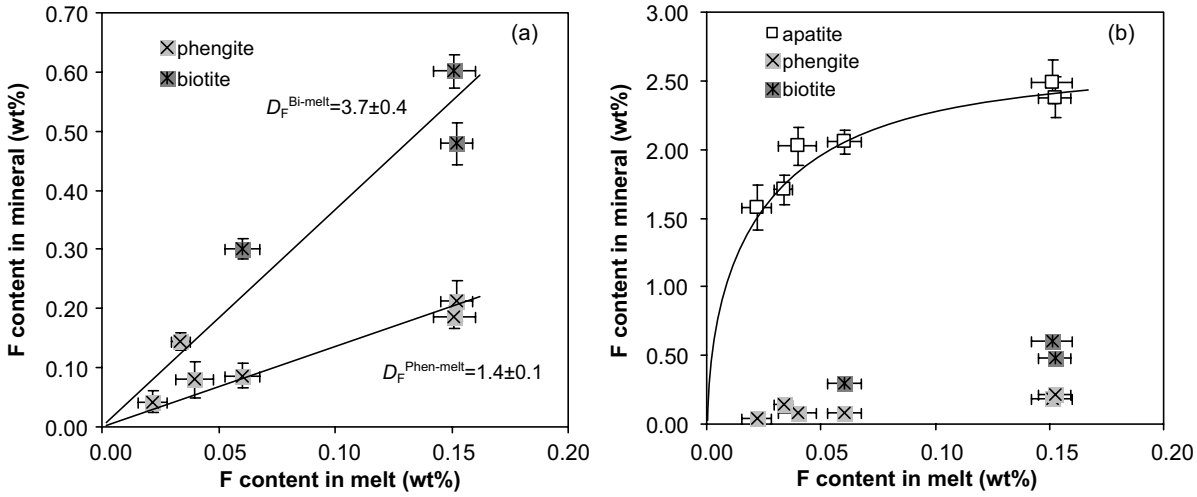
(a)
phengite
biotite
$D_F^{Bi\text{-}melt}$=3.7±0.4
$D_F^{Phen\text{-}melt}$=1.4±0.1
F content in mineral (wt%)
F content in melt (wt%)
0.00
0.10
0.20
0.30
0.40
0.50
0.60
0.70
0.00
0.05
0.10
0.15
0.20
(b)
apatite
phengite
biotite
F content in mineral (wt%)
F content in melt (wt%)
0.00
0.50
1.00
1.50
2.00
2.50
3.00
0.00
0.05
0.10
0.15
0.20

Figure 5

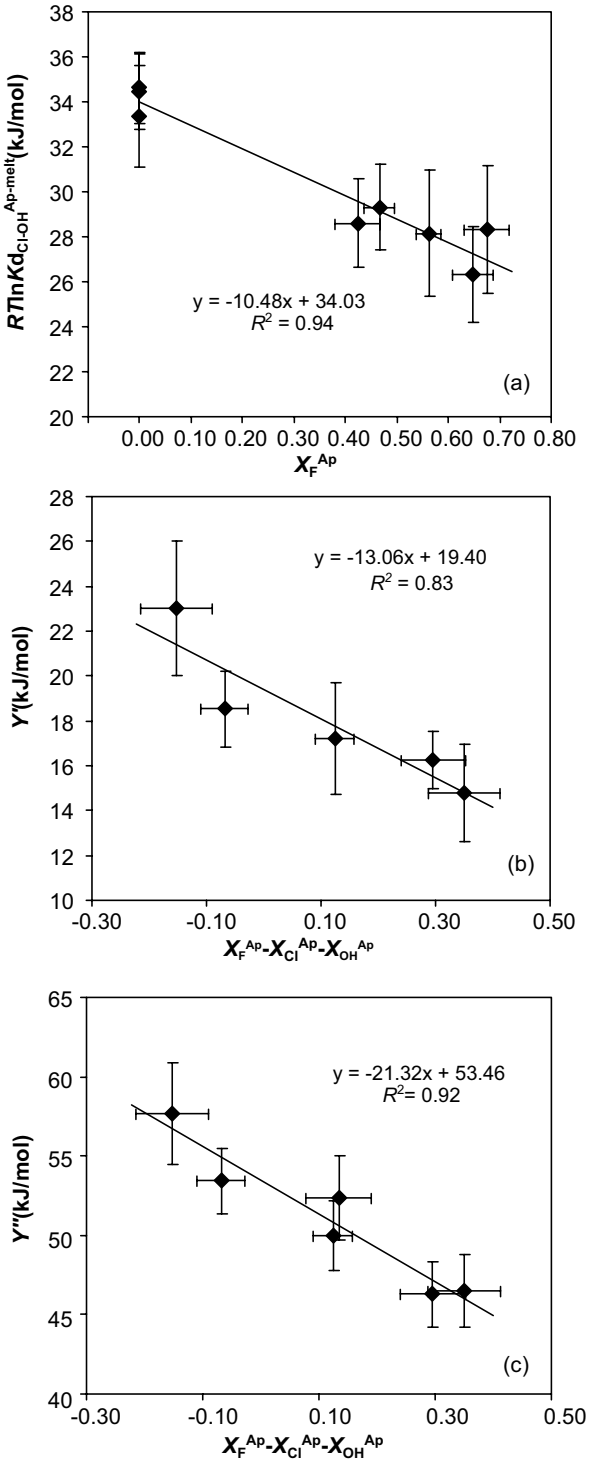
y = -10.48x + 34.03
R^2 = 0.94
(a)
$RT\ln Kd_{Cl\text{-}OH}^{Ap\text{-}melt}$(kJ/mol)
X_F^{Ap}
y = -13.06x + 19.40
R^2 = 0.83
(b)
Y'(kJ/mol)
X_F^{Ap}-X_{Cl}^{Ap}-X_{OH}^{Ap}
y = -21.32x + 53.46
R^2= 0.92
(c)
Y''(kJ/mol)
X_F^{Ap}-X_{Cl}^{Ap}-X_{OH}^{Ap}

Figure 6

This is a preprint, the final version is subject to change, of the American Mineralogist (MSA)
Cite as Authors (Year) Title. American Mineralogist, in press.
(DOI will not work until issue is live.) DOI: http://dx.doi.org/10.2138/am-2017-5891

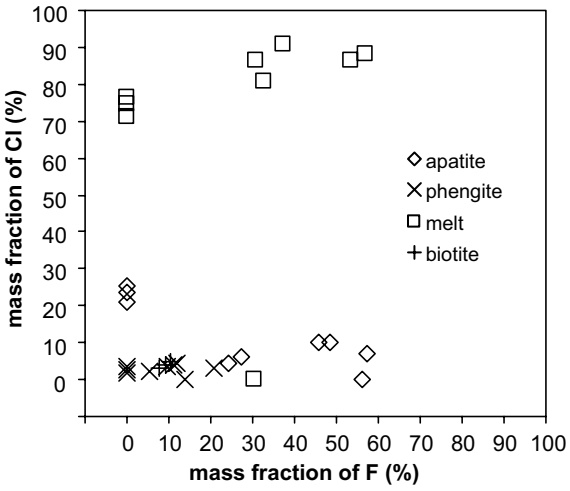

Figure 7

This is a preprint, the final version is subject to change, of the American Mineralogist (MSA)
Cite as Authors (Year) Title. American Mineralogist, in press.
(DOI will not work until issue is live.) DOI: http://dx.doi.org/10.2138/am-2017-5891

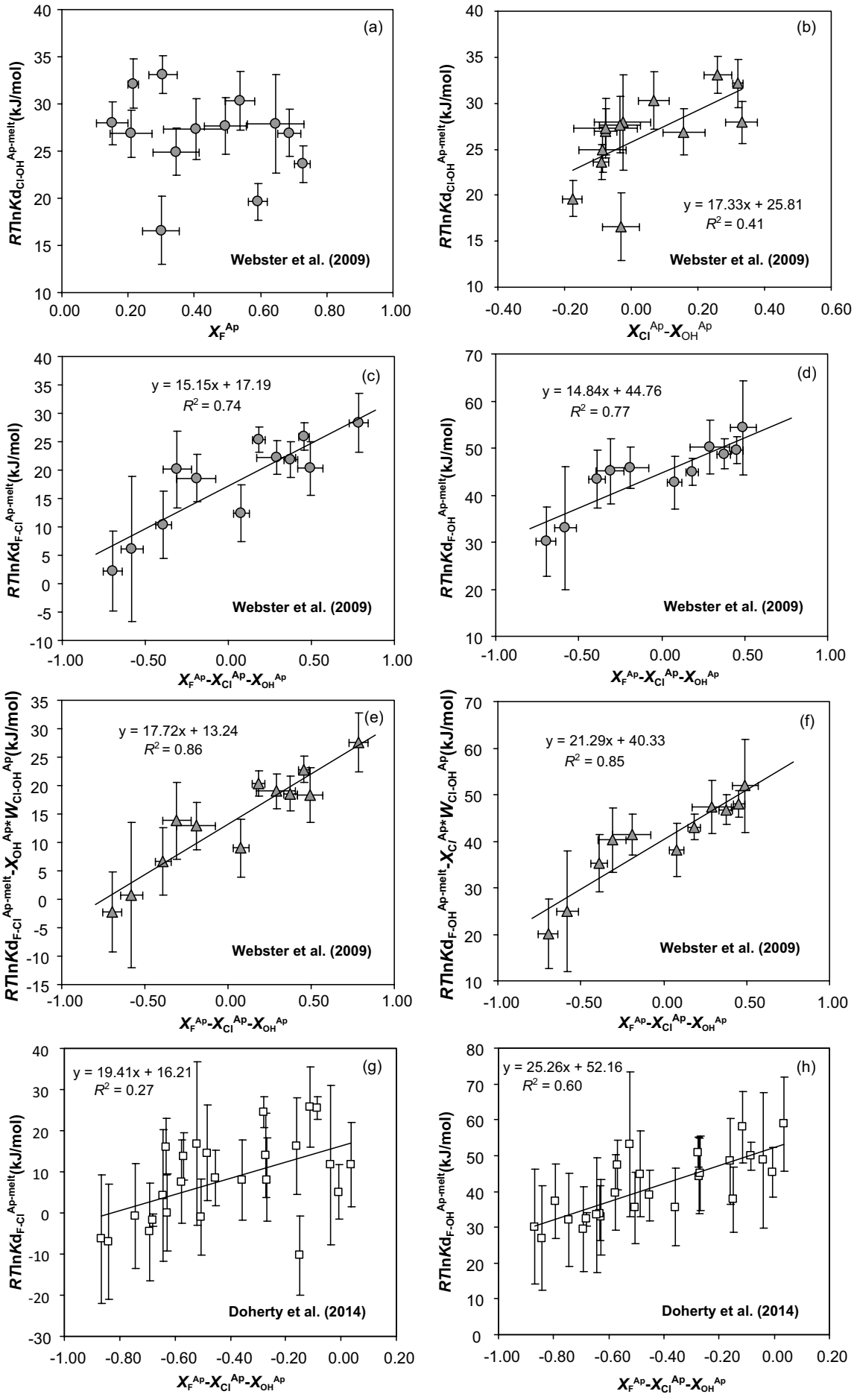

Figure 8

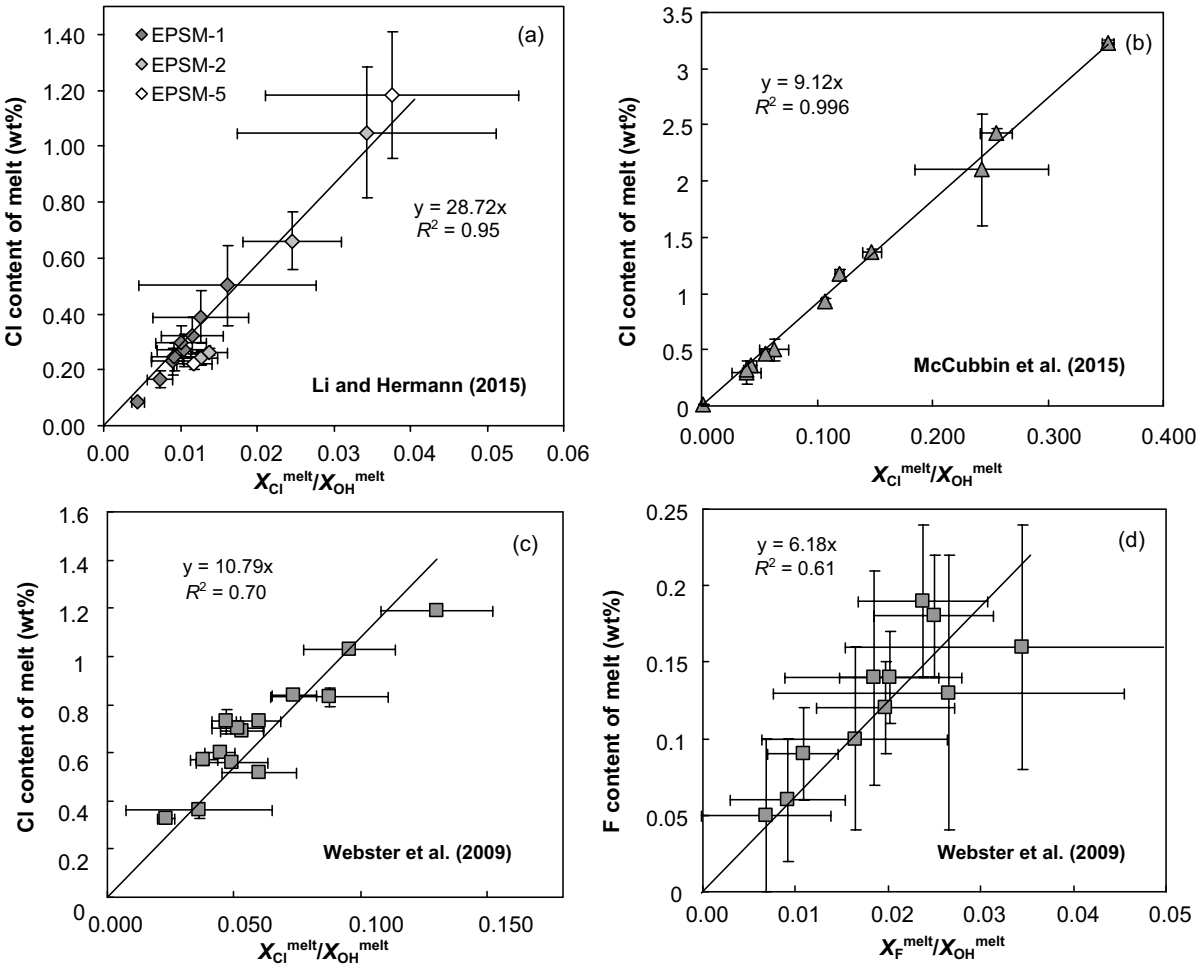
(a)
EPSM-1
EPSM-2
EPSM-5
y = 28.72x
R^2 = 0.95
Li and Hermann (2015)
Cl content of melt (wt%)
$X_{Cl}^{melt}/X_{OH}^{melt}$
(b)
y = 9.12x
R^2 = 0.996
McCubbin et al. (2015)
Cl content of melt (wt%)
$X_{Cl}^{melt}/X_{OH}^{melt}$
(c)
y = 10.79x
R^2 = 0.70
Webster et al. (2009)
Cl content of melt (wt%)
$X_{Cl}^{melt}/X_{OH}^{melt}$
(d)
y = 6.18x
R^2 = 0.61
Webster et al. (2009)
F content of melt (wt%)
$X_{F}^{melt}/X_{OH}^{melt}$

Figure 9

This is a preprint, the final version is subject to change, of the American Mineralogist (MSA)
Cite as Authors (Year) Title. American Mineralogist, in press.
(DOI will not work until issue is live.) DOI: http://dx.doi.org/10.2138/am-2017-5891

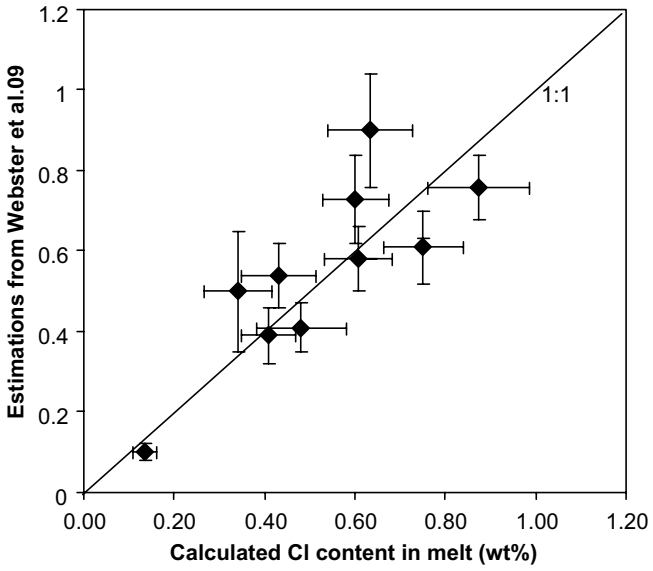

Figure 10